Excitation and charge transfer in low-energy Na^+-Ne collisions

J. Østgaard Olsen and T. Andersen
Institute of Physics, University of Aarhus, DK-8000 Aarhus, Denmark

M. Barat, Ch. Courbin-Gaussorgues, V. Sidis,* J. Pommier, and J. Agusti
Laboratoire des Collisions Atomiques et Moléculaires, Université de Paris-Sud, F-91405 Orsay Cedex, France

N. Andersen and A. Russek†
Physics Laboratory II, H.C. Ørsted Institut, DK-2100 Copenhagen, Denmark and NORDITA, Blegdamsvej 17, DK-2100 Copenhagen, Denmark

(Received 5 July 1978)

This work presents a multifaceted experimental and theoretical study of collisions of Na^+ ions in the energy range 0.2–12 keV with Ne atoms. Four different collision experiments are reported here. With one, doubly differential cross sections in scattering angle and energy loss were obtained by electrostatic analysis for direct collisions in the energy range 0.5–3.0 keV. With a second, energy-loss spectra for the neutral component of the scattered beam were obtained by time-of-flight techniques. With a third, energy spectra of electrons ejected by autoionization decays were obtained in the impact energy range 0.5–12 keV. Finally, in a fourth experiment, cross sections were obtained for some important Ne II transitions excited by collisions in the energy range 0.2–10 keV. The results of these four experiments are combined with results from previous investigations to give detailed information on the relative role of the various one- and two-electron excitation processes. The interpretation of the experimental findings is carried out within the quasimolecular framework and is based on the results of *ab initio* calculations for a variety of potential-energy curves of the $(Na\text{-}Ne)^+$ quasimolecule. It is shown that the observed processes are induced by a succession of independent transition mechanisms, namely, (i) primary single and double excitation of Ne $2p$ electrons at curve crossings of the $4f\sigma$ molecular orbital with empty σ orbitals, (ii) $\sigma \rightarrow \pi$ population transfer via rotational coupling, (iii) core rearrangement processes (L-vacancy sharing), and finally (iv) outer-electron (Rydberg) sharing. The estimation of the importance of the different mechanisms is made using simple models (Landau-Zener, Demkov-Meyerhof) and extrapolations of previous theoretical and experimental results on the isoelectronic Ne-Ne system. Special attention has been focused on the production of Ne $(2p^5 3p)$ triplet states, where it is demonstrated that simultaneous excitation of both target and projectile can well account for the Ne triplet excitation without invoking a breakdown of the Wigner spin-conservation rule.

I. INTRODUCTION

A. Scope and motivation

In this work, the results of four different experiments as well as a theoretical study are reported on collisions of Na^+ ions with Ne atoms in the impact energy range 0.2–12 keV. The experiments are: (i) and (ii) doubly differential cross sections in scattering angle and energy loss for both charged and neutral scattered sodium; (iii) energy spectra of the electrons ejected from autoionizing decay of doubly excited final states; and (iv) cross sections for photon emission from important final states.

These are all components of a combined experimental and theoretical investigation of the energy levels of the $(Na - Ne)^+$ molecular system and of the couplings between these levels. The rather extensive overall effort is both justified and indeed necessary. Neither the theory alone (with a realistic amount of effort) nor any single experimental study could provide the qualitative and quantitative understanding of the $(Na - Ne)^+$ energy levels obtained by the combined approach. In fact, because of the understanding of the molecular-ion system thus obtained, some misinterpretations which have appeared in the literature are corrected. The misinterpretations were all due to attempts to draw inferences from only one aspect of the collision.

The reason why the $(Na - Ne)^+$ system requires such an extensive effort is that it is *not* a simple system displaying essentially just one of the well-known mechanisms (such as $2p\sigma$-$2p\pi$ rotational coupling, or the Rosenthal effect, or Demkov coupling), and is therefore *not* accessible to one single appropriate technique. Rather, it is a complicated many-channel system for which the entire zoological garden of different mechanisms are active at various internuclear distances and the study of which requires several experimental techniques all working together to make a consistent interpretation possible.

It is, of course, possible *in principle* to determine molecular energy levels for any given system directly from *ab initio* calculations, without the

help of experiment. However, practical limitations both on computer capacity and financial resources would have rendered the *ab initio* calculations either prohibitive or lacking the required accuracy, if done alone. Without the experimental input indicating the important configurations, the *ab initio* calculations could not have been undertaken. Indeed, an early molecular calculation in this study associated the two-electron excitations with the wrong level crossing. Moreover, after the calculations are completed, the experimental data subsequently provide a comprehensive check on the accuracy of these calculations both with regards to locations of level crossings, the energies at which they intersect, the slopes of the diabatic curves at the crossings, and even the strengths of some of the couplings at the crossings.

On the experimental side, what is needed to investigate the molecular potential curves of a scattering system is a set of differential cross sections for various channels following these potential curves. The task is complicated, however, by the limited energy resolution of the differential scattering technique, which most often does not allow an identification of the specific final states, but only a determination for the two groups of levels corresponding to one- and two-electron excitation. Thus, in order to infer the differential scattering cross section which results when the system follows specified molecular potential curves on the incoming and outgoing portions of the trajectory, differential energy-loss spectra must be supplemented by cross sections for photon emission and electron ejection as functions of the respective energies. Even then, a considerable amount of detective work is required.

From the theoretical point of view our understanding of the mechanisms responsible for excitations produced by heavy-particle collisions has rapidly progressed in recent years, thanks to the development of the quasimolecular picture. The present detailed experimental study offers an opportunity to further test this theoretical approach. For accurate quantitative results molecular *ab initio* calculations are necessary to locate curve crossings (related to cross-section thresholds) with precision and as well to determine the shape of the energy curves, their relative position, and interaction between the relevant molecular states. However, the efficiency of the different mechanisms can easily be checked using simple models without attempting the full solution to the quantal close-coupling scattering equations. It is in fact shown that one can build a consistent overall interpretation which is both qualitatively and semiquantitatively correct with modest computational machinery.

B. Historical perspective

The alkali-metal-ion–rare-gas collisions have played an important role in the early history of atomic collision studies. Systematic investigations of alkali-metal-ion–rare-gas interactions were taken up in the late 1920s in Ramsauer's laboratory, where the elastic part of the interatomic potentials (<60 eV)[1] and the ionization processes were studied. At the same time the ionization process was studied extensively in Millikan's laboratory. These latter experiments yielded two unexpected results: (a) a quasisymmetry effect and (b) a sharp threshold for ionization. The quasisymmetry effect showed that "Ionization of a noble gas is best effected by that alkali ion closest to it in mass or number of electrons."[2] By studying the Z dependence it was concluded that this was not just a mass effect, but a question of electronic configuration. The sharp energy threshold for ionization was found to be much higher than required from energy conservation alone, and was interpreted by Weizel and Beeck[3] in terms of a quasimolecular picture. They suggested that in the case of Na^+-Ne the $4f\sigma$ promotion gives rise to a crossing between the incoming ground-state potential curve and an outgoing curve leading to ionization; this curve was believed to correspond to a doubly excited state which autoionizes later on. This in turn inspired Stueckelberg's detailed theoretical investigation[4] of the curve-crossing problem, and his analysis of the K^+-Ar collision showed good agreement between theory and experiment. A lucid account of this development is given in Beecks review paper[5] of 1934. Studies of the optical radiation from the alkali-metal-ion–rare-gas collisions were taken up around 1936 by Maurer[6] but unfortunately in a less systematic way. His investigations did not include the Na^+-Ne system which is the main concern of the present work.

More than thirty years elapsed—during which time most of the early findings were forgotten—before this class of collision systems again became subject for intensive studies. During the last decade several, mainly experimental, papers have appeared, treating different aspects of these collisions, including differential-scattering measurements and electron and photon spectroscopy. The main results of previous investigations of the Na^+-Ne system will be included in the discussion in the following sections.

The goal of this paper is a unified picture of the experimental findings and a theoretical understanding of the capture and excitation porcesses for the Na^+-Ne system. Mouzon from Millikan's laboratory stated in 1932, in a paper on alkali-metal ions colliding with rare gases, that "The problem

of the ionization of gases by impact of positive ions at low velocities is one in which it is necessary for a large amount of experimental evidence to be gathered before the theorist is able to hazard an intelligent guess of the processes involved."[7]

C. Outline of the investigation

Following a brief description of the various experimental approaches used in this investigation (Sec. II), results are presented of a series of experiments carried out in our laboratories: The impact-parameter dependence of the three main groups of processes (i) elastic, (ii) one-electron excitation, and (iii) two-electron excitation is displayed by the differential-scattering results (Sec. III). Detailed information on the distribution of excitation within the different excited levels of the latter two groups is obtained from electron spectroscopy (Sec. IV) and photon spectroscopy (Sec. V). The relative importance of the various excitation processes is analyzed in Sec. VI, including also results of previous experimental and theoretical investigations. Theoretical calculations, including computation of molecular potential curves and scattering calculations, are presented in Sec. VII. It will be seen that the basic interpretation of Weizel and Beeck[3] of the primary mechanisms responsible for excitation are found to be valid, but due to more refined experimental techniques and more powerful theoretical tools, the understanding of the excitation processes and their relative role will be put on a much more rigorous basis.

II. EXPERIMENTAL APPROACHES

A. Collision spectroscopy

Differential-scattering measurements have been performed in the 0.5–3.0 keV energy range using two different apparatuses, a collision spectrometer with electrostatic analysis (ESA) and a time-of-flight spectrometer (TOF). Since both devices have been described in considerable detail elsewhere only brief descriptions will be given here.

The ESA spectrometer[8] consists of a low-energy (0.1–15 keV) accelerator[9] and a differential-scattering chamber.[10] The Na^+ ions are produced from NaCl in a universal ion source, using a separate oven for evaporation of the NaCl. The ions are extracted and focused into a beam which, in turn, is mass analyzed in a magnet before deceleration to the desired energy. The beam enters the scattering cell, containing neon at low pressure (0.1–1 mTorr) through a pair of circular collimating apertures. Ions scattered through an angle θ are selected by a system of slits. Their energy is determined by an electrostatic analyzer, after which they are detected by a channeltron electron multiplier. The angular resolution of the apparatus was about 0.3°.

The main features of the scattering chamber have been described in detail by Fastrup *et al.*[10] In order to improve the energy resolution, the original analyzing system has been modified to allow deceleration of the scattered ions prior to analysis. An energy-loss spectrum is obtained by sweeping the deceleration voltage about some mean value, keeping the analyzer voltage fixed.

Measurements of the differential cross section for charge transfer as well as the total differential-scattering cross section (i.e., the cross section for scattering through a specific angle, irrespective of state of charge and excitation) have also been performed with this apparatus by replacing the electrostatic analyzer by a pair of deflection plates followed by a channeltron. By applying a voltage to the deflection plates, the scattered ions are swept away so that only the neutrals are detected. With the plates grounded all particles are detected.

The time-of-flight spectrometer has been described in detail by Brenot *et al.*[11] Few modifications have been made for this particular experiment. The discharge ion source has been replaced by a Na^+ thermionic ion emitter commercially available from Spectra-Mat, Inc. and of the same type as the Li^+ ion source described by Heinz and Reaves.[12] The ion beam is focused and, after being "chopped" into nanosecond pulses by an rf electric field, enters the collision cell containing the Ne target gas. Before reaching the detector, the scattered particles pass through an electric deflecting field which permits selection of ions plus neutrals (field turned off) or the neutrals only (field turned on). A time to amplitude converter (TAC) is used to perform the TOF analysis. The output of the TAC is pulse-height analyzed and stored in a multichannel analyzer. For each angle two TOF spectra are recorded, one for neutrals and one for ions. (The ion spectrum is obtained by subtracting the spectrum of neutrals from the spectrum of neutrals plus ions.)

For small scattering angles a typical energy resolution of 2 eV at 1 keV was achieved in the present experiment. However, the resoltuion at the angles of main interest here ($\theta \gtrsim 7°$ at 1 keV) is deteriorated by the effects of the thermal motion of the target and the limited angular resolution ($\Delta\theta \simeq 0.2°$).[13] The zero angle has been determined within ±0.05°.

B. Electron spectroscopy

The electron emission from Na^+-Ne collisions have been studied in the range of projectile energies 0.5–12 keV. The Na^+ beam is collimated by a pair of circular apertures before entering the collision cell containing Ne at a pressure of about 1 mTorr, which is low enough to ensure single-collision conditions. Electrons emitted from the collision center at an angle θ_e with respect to the incident beam direction are energy analyzed by a 60° cylindrical electrostatic analyzer having an energy resolution of $\Delta E/E = 0.018$. Some measurements were performed with improved resolution obtained by deceleration of the electrons before analysis. The observation angle θ_e can be varied continuously between 20° and 160°.

A detailed description of the spectrometer and of kinematical effects associated with electron spectroscopy of ion-atom collisions have been given by Dahl *et al.*[14]

C. Optical spectroscopy

The apparatus used for the optical measurements has been described previously.[9] The ion beam from the accelerator passes through a differentially pumped collision cell containing the target gas at low pressure. The light emitted from the collision region is viewed perpendicular to the beam by a spectrometer. In the visible region of the spectrum, a 0.3-m McPherson model 218 spectrometer equipped with a dry-ice cooled EMI 6256 S photomultiplier tube was used to analyze and detect the emitted light. The light polarization could be measured with a rotatable linear polarizer placed in the light path between the collision cell and the spectrometer. For the uv measurements a 0.5-m Seya-Namioka spectrometer (McPherson model 235) equipped with a Bendix channeltron detector 33029 was used. Standard pulse-counting technique was applied throughout the measurements.

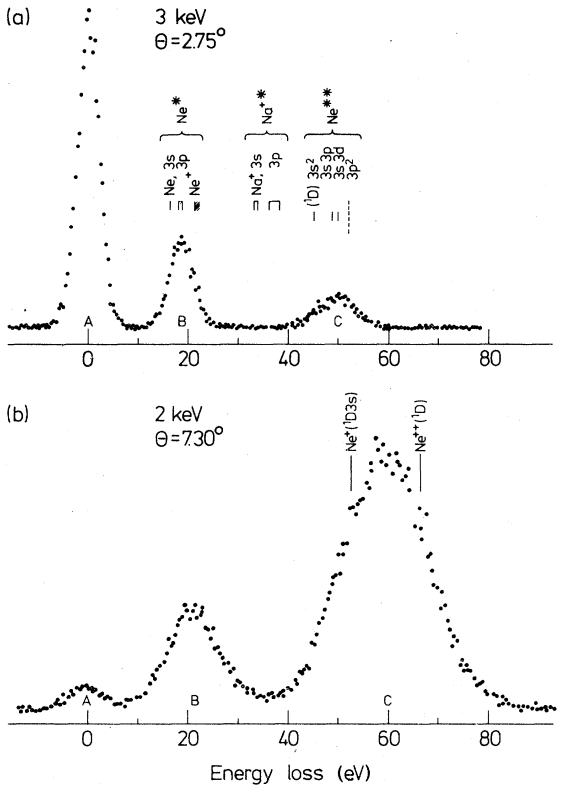

FIG. 1. Energy-loss spectra of scattered Na^+ ions from Na^+-Ne collisions. The spectra are obtained by electrostatic analysis. Peaks *A*, *B*, and *C* correspond to elastic scattering and scattering with one- and two-electron excitations, respectively. (a) shows the dominance of the Ne($2p^5 3p$) excitation for one-electron excitation, and Ne($2p^4(^1D)n\,l'l'$) for two-electron excitation. (b) Shows the importance and marked broadening of the *C* peak at larger scattering angles

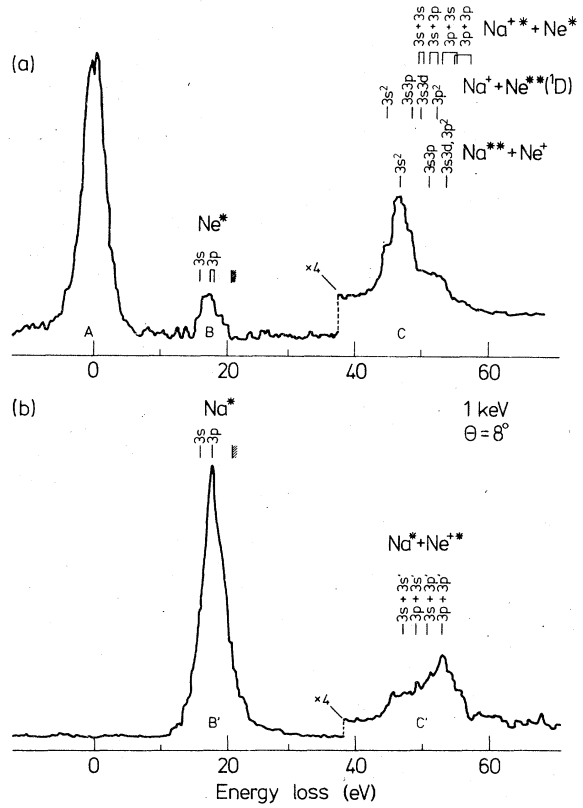

FIG. 2. Energy-loss spectra obtained by time-of-flight analysis of scattered Na^+ ions (a) and neutrals (b) from Na^+-Ne collisions. (a) shows the importance of the Ne($2p^5 3p$) state in the *B* peak. (b) Peaks *B'*, *C'*, correspond to one-electron charge transfer and to charge transfer with simultaneous Ne^+ excitation, respectively, with a clear dominance of the Na($2p^6 3p$) state in the *B'* peak.

III. DIFFERENTIAL-SCATTERING RESULTS

A. Energy-loss spectra

Typical energy-loss spectra, both ESA (ion spectra) and TOF (ion and neutral) are shown in Figs. 1–3. The ion spectra (Figs. 1 and 2) show the distribution of energy losses for beam particles (Na^+) scattered without change of charge state. The spectra all exhibit the well-known triple-peak structure already observed by Afrosimov *et al.*[15] for this collision.

Of the three peaks observed, A corresponds to elastic scattering, B to one-electron excitation of Ne, and C to either two-electron excitation of Ne or simultaneous excitation of Na^+ and Ne. The energies of the most important exit channels are listed in Table I.

The following features of the spectra should be noticed: In the B peak the Ne($3p$) state appears to be dominant and the Ne($3s$) state relatively weak. A similar observation was made by Brenot *et al.*[16] for the isoelectronic Ne-Ne system. Higher excited states of Ne and ionization of Ne may also contribute to the B peak but no "ionization tail" is observed so "direct" ionization of Ne seems to be relatively weak as is also the case in the Ne-Ne system.[16]

As seen from Fig. 1(b), the two-electron excitation peak C becomes dominant in the spectra for violent collisions. It moves towards higher energy-loss values and becomes very broad; many different two-electron processes (Table I), among those also the ionization processes $Na^+ + Ne^{+*} + e^-$, can give rise to energy losses in this region. A more detailed discussion of the two-electron processes will be given in Sec. IV in connection with the electron-spectroscopy results.

No excitation of the Na^+ ion without simultaneous excitation of Ne ($\Delta E \simeq 32.9$–47.3 eV) has been observed in the present measurements. This behavior contrasts with that of the superficially similar K^+-Ar system for which strong excitation of K^+ has been observed by Afrosimov and collaborators.[15,17] This will be commented upon in Sec. VII C.

The TOF spectra of neutrals [Figs. 2(b) and 3] show the distribution of energy losses for Na^+ ions which have captured an electron from the neon target during the collision. Two peaks are seen in the spectra. The first one (B') corresponds to electron transfer with the Ne^+ ion remaining in its ground state. Capture to the Na($3p$) excited state seems to be the dominant channel whereas capture to the Na($3s$) ground state appears to be weaker. The second peak (C') is ascribed to capture into the Na($3s$) ground state or the Na($3p$) excited state with simultaneous excitation of Ne^{+*}.

Figure 3 shows the neutral spectra as functions of angle at 2-keV beam energy. Again one observes that the importance of the two-electron peak (C') increases as the collisions become more violent. For large scattering angles the capture plus ionization channels $Na^{(*)} + Ne^{2+} + e$ contributes significantly to the C' peak.

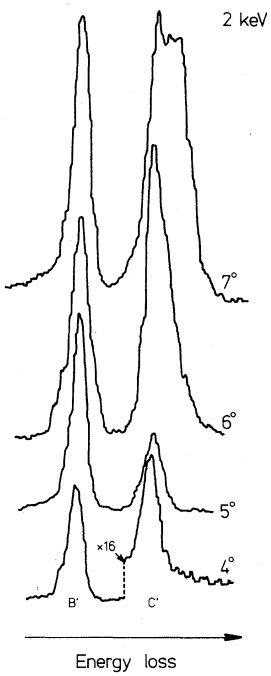

FIG. 3. Energy-loss spectra of scattered Na neutrals from Na^+-Ne collisions at various angles. The spectra are obtained by TOF technique. Peaks B', C' correspond to one-electron charge transfer and to charge transfer with simultaneous Ne^+ excitation, respectively. The importance of the C' peak is seen to increase with increasing scattering angle.

B. Differential cross sections

The differential cross sections (DCS) for the various processes have been obtained by the following procedures: For a given energy, energy-loss spectra have been recorded at a number of different angles using the ESA spectrometer described in Sec. II, and the areas of the peaks in these ion spectra were then determined by planimetry. The total differential-scattering cross section and the "total" differential charge-transfer cross section were also measured with the ESA apparatus modified as described in Sec. II. Using the ratio between the B' and C' processes determined from the TOF spectra, the "total" charge-transfer DCS were resolved to give the DCS for the B' and C' processes separately (see Fig. 4). The DCS are presented in reduced units, i.e., the reduced cross section $\rho = (d\sigma/d\Omega)\,\theta \sin\theta$ is plotted versus the reduced angle $\tau = E\theta$. At τ values smaller than ~7 keV deg the measurements show that the scattering is purely elastic (i.e., only peak A appears in the ion spectra and no neutrals are detected). In this τ region the reduced cross section is a function of τ only (i.e., independent of energy)

TABLE I. Energy defects of the various exit channels discussed in the text. Energies of optical levels are taken from C. E. Moore's tables of Atomic Energy Levels (NBS Circular 467). Energies of autoionizing levels can be found in Refs. 22–25. The direct and exchange one-electron processes give rise to, respectively, peaks B and B' in the energy-loss spectra, Figs. 1 and 2. The direct and exchange two-electron processes give rise to, respectively, peaks C and C', with one exception: exchange processes populating doubly excited sodium levels will contribute to the C peak because these levels autoionize before detection.

	Core states	Outer electrons direct (D) or exchange (E)	Exit channel	Energy defect (eV)
		–	$Na^+ - Ne$	0.00
$1e^-$ processes	$Na^+ + Ne$	E	$Na(3s) - Ne^+$	16.43
			$Na(3p) - Ne^+$	18.53
		D	$Na^+ - Ne(3s)$	16.67–16.85
			$Na^+ - Ne(3p)$	18.38–18.96
			$Na^+ - Ne^+ + e^-$	21.56
	$Na^{2+} + Ne$	D	$Na^+(3s) + Ne$	32.84 – 33.32
			$Na^+(3p) + Ne$	36.35 – 38.29
$2e^-$ processes	$Na^+ + Ne^{2+}$	D	$Na^+ + Ne^{**}(^1D)3s^2\,^1D$	45.15 ± 0.05
			$Na^+ - Ne^{**}(^1D)[3s3p(^1P)]$	48.90 ± 0.05
			$Na^+ - Ne^{**}(^1D)[3s3d(^1D)]$	50.05 ± 0.05
			$Na^+ - Ne^{**}(^1D)[3p^2(^1S, ^1D)]$	52.35 ± 0.05
		E	$Na(3s) + Ne^+(^1D3s)$	46.97
			$Na(3p) + Ne^+(^1D3s)$	49.07
			$Na(3s) + Ne^+(^1D3p)$	50.44–50.80
			$Na(3p) + Ne^+(^1D3p)$	52.54–52.90
			$Na(3s) + Ne^+(^1D3d)$	54.28–54.74
			$Na(3p) + Ne^+(^1D3d)$	56.38–56.84
		D	$Na^+ + Ne^+(^1D3s) + e^-$	52.11
			$Na^+ + Ne^+(^1D3p) + e^-$	55.58–55.94
			$Na^+ + Ne^{2+}(^1D) + 2e^-$	62.64
	$Na^{2+} + Ne^+$	E	$Na^{**}(2p^5 3s^2) + Ne^+$	47.25 ± 0.05
			$Na^{**}(2p^5 3s3p) + Ne^+$	51.35 ± 0.05
			$Na^{**}(2p^5, 3p^2$ or $3s3d) + Ne^+$	54.05 ± 0.05
		D	$Na^+(3s) + Ne(3s)$	49.51 – 50.17
			$Na^+(3s) + Ne(3p)$	51.22 – 52.28
			$Na^+(3p) + Ne(3s)$	53.02 – 55.14
			$Na^+(3p) + Ne(3p)$	54.71 – 57.25
		–	$Na^{2+} + Ne^-(2p^5 3s^2)$	63.30
			$Na^{2+} + Ne^+ + 2e^-$	68.86

according to the scaling principle of Smith *et al.*[18] Relative cross sections measured at different energies can therefore be normalized together at small τ values and brought on an absolute scale by comparison with the elastic cross section calculated from a known elastic potential. For this purpose of normalization we have chosen the potential of Kita *et al.*,[19] derived from elastic scattering data (see also Sec. VII B). The normalization procedure described above is necessary since the efficiency of the scattered particle detectors is not known with sufficient accuracy at these low energies.

The reduced DCS for all processes at 2 keV are shown in Fig. 5. Almost constant at small τ values, the elastic cross section (A) drops off sharply at about 9 keV deg reflecting the opening of inelastic channels. The one-electron cross sections, i.e., the cross section for single-electron excitation of Ne (B) and the cross section for charge transfer without Ne^+ excitation (B') are rather similar. After a sharp onset, they reach a maximum and then fall off, exhibiting pronounced oscillations during the decrease. However, the primary maximum in the B' DCS is generally larger than the corresponding B maximum and appears at a somewhat (~1 keV deg) lower value of τ.

The two-electron cross sections C and C' appear at slightly higher values of τ than the corresponding one-electron cross sections. For large τ they

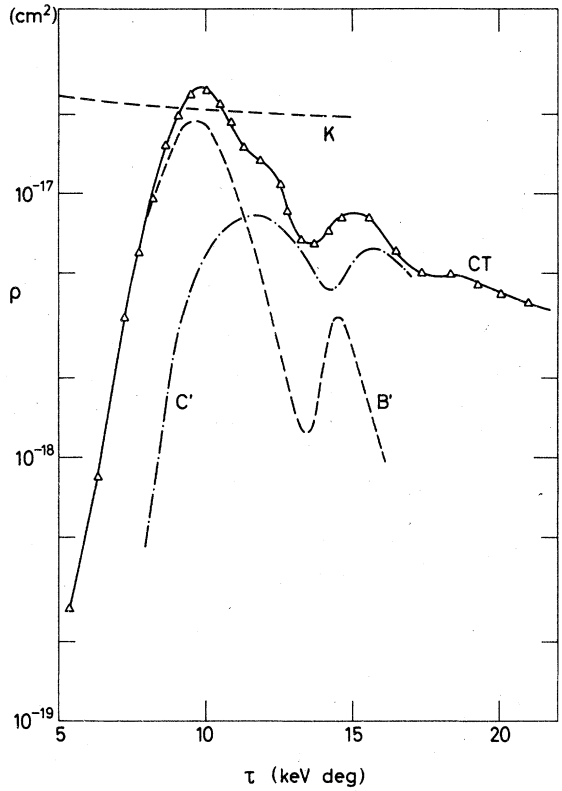

FIG. 4. Resolution of the differential charge-transfer cross section (CT) in its two components: charge transfer without Ne^+ excitation (B') and charge transfer with simultaneous Ne^+ excitation (C'). The curve labeled K represents the elastic cross section (see text) used for calibration.

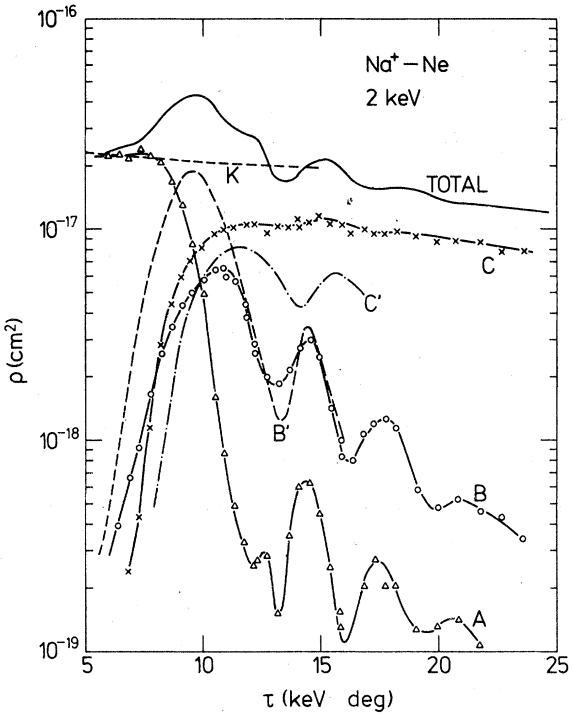

FIG. 5. Reduced differential cross sections for Na^+-Ne collisions at 2-keV beam energy as a function of reduced scattering angle. The same notation is used as in Figs. 1–4. The curve labeled K represents the elastic cross section (see text) used for calibration. The curve labeled TOTAL represents the total differential scattering cross section.

decrease very slowly and display only a weak undulatory structure.

The similar behavior of the DCS's for direct excitation and charge-transfer processes, for both one- and two-electron excitation, suggests a common mechanism for the population of these channels.

As seen from Fig. 5, the total differential-scattering cross sections are strongly perturbed by the opening of the inelastic channels. This phenomenon is discussed in detail in Sec. VIIE.

In Fig. 6 is shown the elastic DCS for a number of different energies. In both the purely elastic region ($\tau < 7$–8 keV deg) and in the fall-off region ($8 \lesssim \tau \lesssim 11$ keV deg), the curves are almost identical, showing that it is the impact parameter $b \times [b = b(\tau)$ (Ref. (18)], and not the energy which mainly characterizes the excitation mechanism. The oscillations and the strong absorption seen in the elastic cross section at large τ values have previously been observed in several other systems.[15-18,20]

The threshold for the reduced DCS's for one-electron excitation of Ne (process B), shown in Fig. 7, is seen to be almost energy independent. Also the value of the first maximum is only weakly dependent on energy, whereas the period of oscillation is found to be proportional to $E^{1/2}$. This behavior of the cross sections shows that the inelastic processes are due to curve crossings within a narrow interval of internuclear distance of the incoming channel with channels leading to excited states. The $E^{1/2}$ dependence of the oscillation period is characteristic of a Stueckelberg oscillation, to be discussed further in Sec. VIE.

C. Integrated cross sections

Total inelastic cross sections Q have been obtained from the inelastic differential cross sections by use of the formula

$$Q = 2\pi \int_0^{E\pi} \frac{\rho(\tau)}{\tau} d\tau .$$

Curves of $\rho(\tau)/\tau$ vs τ obtained from the data in Fig. 5 are shown in Fig. 8. The areas below the curves have been determined by planimetry.

It should be noted that the dominant contribution to the one-electron cross sections (B, B') comes from a narrow interval of reduced angle ($\Delta\tau \sim 5$

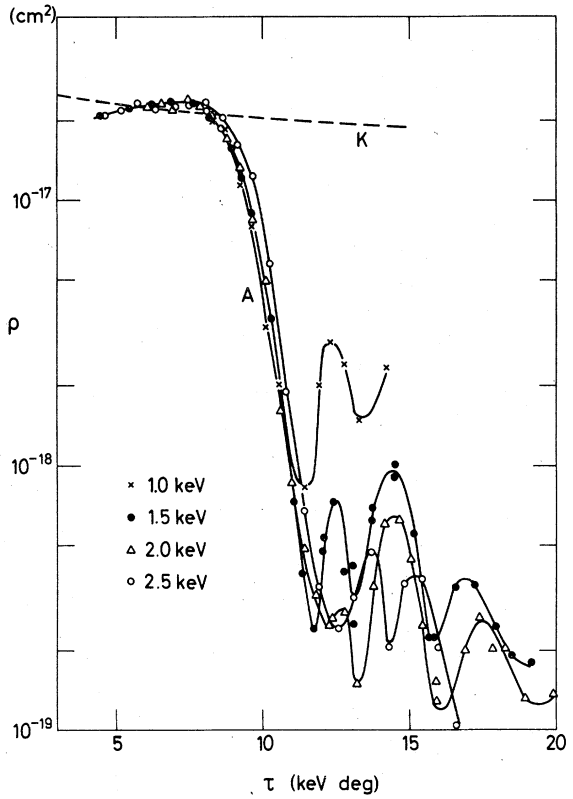

FIG. 6. Reduced differential cross sections for elastic scattering (peak A) as a function of reduced scattering angle at four different beam energies. Curve labeled K represents the elastic cross section used for calibration (see text).

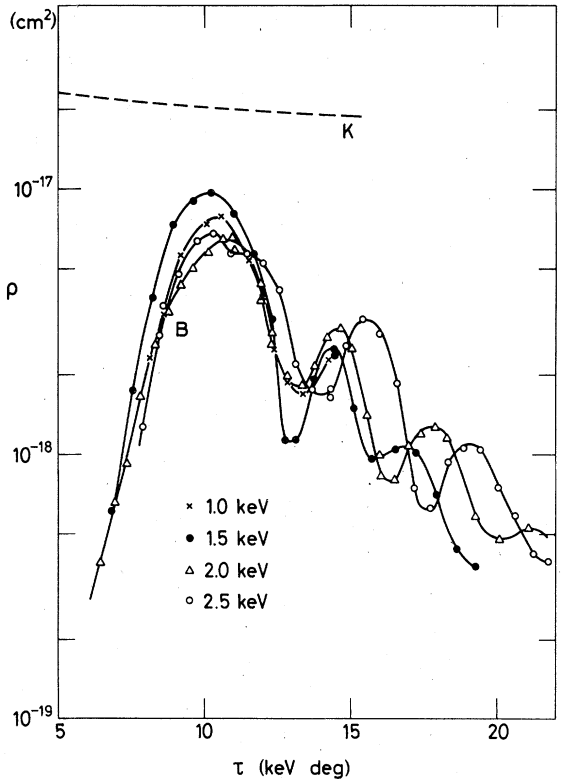

FIG. 7. Reduced differential cross sections for one-electron excitation of Ne (peak B) as a function of reduced scattering angle at four different beam energies. Curve labeled K represents the elastic cross section used for calibration (see text). Pronounced Stueckelberg oscillations are seen.

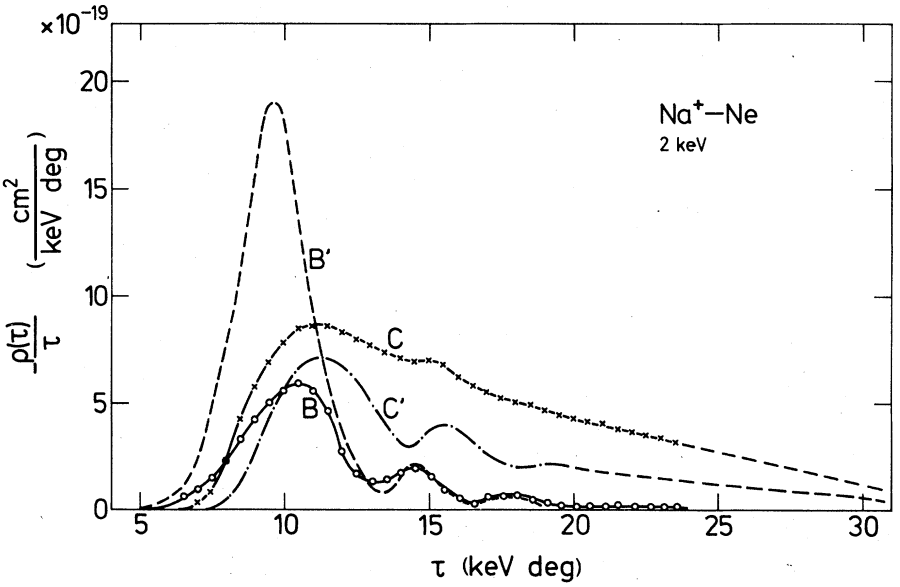

FIG. 8. Reduced differential cross sections divided by reduced scattering angle as a function of reduced scattering angle. Notations as in Figs. 1–4. Extrapolations are shown by dashed lines at the right-hand side of the figure.

TABLE II. Integrated differential cross sections, in units of 10^{-17} cm^2, at various energies of the incident beam. The numbers are obtained in the way illustrated in Fig. 8.

Incident beam energy (keV)	1.0	1.5	2.0	2.5
One-electron excitation (peak B)	1.8	2.4	1.8	2.3
Two-electron excitation (peak C)	3.6	5.3	6.7	7.4
One-electron capture (peak B')	4.0	•••	4.1	•••
Capture + target exc. (peak C')	4.5	•••	3.7	•••

keV deg) around the primary maximum and that the contribution from reduced angles larger than 20–25 keV deg is small.

However, the two-electron excitation curves C, C' in Fig. 8 keep a significant value up to the highest τ values studied in this experiment. An extrapolation of the curves to high τ values is therefore necessary in order to obtain total cross sections for these processes. The extrapolations have been performed linearly as shown in Fig. 8 to yield the cross sections listed in Table II. The linear extrapolation probably underestimates the "tails" of the curves so the total cross sections for the two-electron processes (C, C') in Table II may be too low by as much as 50%–100% whereas the uncertainty of the one-electron cross sections B, B' is probably not larger than 10%–20%.

A detailed discussion of the magnitudes of these cross sections relative to cross sections obtained by other methods is given in Sec. VI.

IV. ELECTRON SPECTROSCOPY

Electron spectroscopy for the Na^+-Ne system has previously been reported by Bydin and collaborators[21] in the region from threshold up to 1-keV impact energy at an observation angle of 90°. Since the Doppler broadening of the lines is most severe at low beam energies and observation angles close to 90°, Bydin *et al.* were only able to resolve a few lines. Due to the more favorable experimental conditions (higher beam energies and smaller observation angles) and to the better energy resolution of our analyzer, we have been able to resolve the individual lines. Furthermore, projectile lines can be distinguished from the target lines by observing the Doppler shift when the observation angle is varied. Bydin *et al.* assigned the observed lines to excitation of $2s2p^6nl$ configurations in neon. Spectra recorded with higher resolution together with an analysis of the MO diagram showed, however, that the lines are actually due to two-electron excitation.[22]

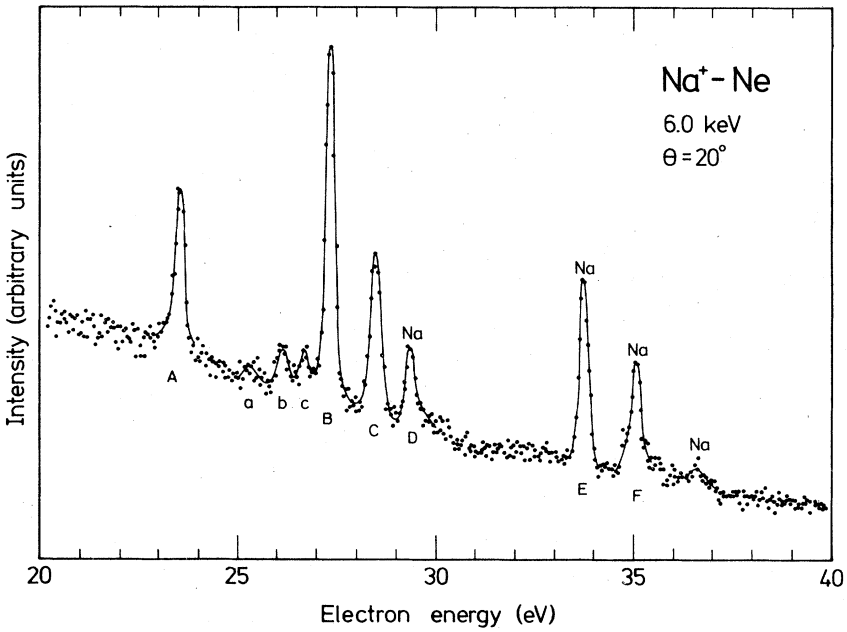

FIG. 9. Electron spectrum for 6-keV Na^+-Ne collisions. The observation angle is $\theta = 20°$. The lines labeled Na arise from autoionizing states in neutral sodium. The other lines belong to neon. Identifications are as follows: Lines A, B, and C are due to decays of the doubly excited levels $1s^2 2s^2 2p^4(^1D)nln'l'$ with $nln'l' = 3s^2\,^1D$, $[3s3p(^1P)]$ and $[3s3d(^1D)]$, respectively. The weak lines a, b, and c arise from $1s^2 2s^2 2p^4(^3P)nln'l'$ levels with $nln'l' = [3s4s(^3S)]^1P$, $[3s3d(^3D)]^1L$, and $[3p^2(^3P)]^1L$, respectively. Finally, the lines D, E, and F arise from the $1s^2 2s^2 2p^5 nln'l'$ configurations with $nln'l' = 3s^2$, $3s3p$, and $3s3d$ or $3p^2$.

A. Spectra

Figure 9 shows a typical spectrum, recorded at 6-keV collision energy. The electron observation angle is 20° with respect to the beam direction, which, at this energy, Doppler shifts the projectile lines enough to avoid overlap with the neon lines. Identification of the neon lines have been discussed in Refs. 22. The sodium lines can be identified by comparison with results of recent investigations.[23] The strong lines A, B, and C are all neon lines belonging to the $1s^2 2s^2 2p^4(^1D)$ core with two additional, excited electrons: A, $3s^2\,^1D$; B, $[3s3p(^1P)]$; and C, $[3s3d(^1D)]$, with electron energies of 23.55, 25.55, and 26.10 eV, respectively. The three weak lines, a, b, and c, between A and B are all neon lines belonging to the $1s^2 2s^2 2p^4(^3P)$ core, with the two outer electrons coupled as a triplet, which in turn couples to the core to give a total singlet state: a, $[3s4s(^3S)]\,^1P$; b, $[3s3d(^3D)]\,^1L$; and c, $[3p^2(^3P)]\,^1L$. These lines show up clearly at low energies, but disappear gradually with increasing impact energy. It is important to note that no triplets are observed. The Wigner spin-conservation rule is thus strictly fulfilled in the electron spectra. No neon lines with $1s^2 2s^2 2p^4(^1S)$ core have been observed. The lines D, E, and F are sodium lines with a $1s^2 2s^2 2p^5$ core configuration, plus excited electrons: D, $3s^2$; E, $3s3p$; and F, $3s3d$ or $3p^2$. Their Doppler-corrected energies are 25.7, 29.8, and 31.1 eV, respectively. No lines corresponding to levels with a $2s$ vacancy in neon or sodium have been seen, though they will give rise to lines in this energy range. $Ne^-(2s^2 2p^5 3s^2)$ excitation, giving a line at 16 eV has been observed below 1-keV impact energy. No lines from Ne^+ or Na^+, and no lines with energies higher than the lines shown in Fig. 9 have been seen in this experiment. As will be shown in Sec. VI, excitation of discrete autoionizing states cannot account for all of the large peak C seen in the energy-loss spectra at large-τ values, Fig. 2. There is, however, an important continuum of electrons emitted, as seen in Fig. 9.

B. Cross sections

The cross sections for excitation of all lines indicated in Fig. 9 are shown in Fig. 10, except for the D line because of problems with partial overlap with the B and C lines in most of the energy range. A preliminary account of this part of our investigation has been reported at an earlier occasion.[24] The intensities are measured at an observation angle of 20°, and the cross sections are evaluated assuming isotropic emission. Since this condition was found not to be strictly fulfilled, the absolute magnitude is only accurate within a factor of 2. The low-energy results of Bydin *et al.*[21] for line A, measured at 90°, have been normalized to our curve. A remarkable feature is the drastic onset of the neon $2s^2 2p^4(^1D)\ 3s^2\,^1D$ excitation, line A, slightly above 200 eV. This sharp rise indicates that the transition occurs at a well-localized curve crossing. The following rapid fall-off at higher energies is connected with the opening of other exit channels such as peaks B and C, corresponding to excitation of $3p$ and $3d$ electrons. We notice the complete absence of a line corresponding to $3p^2$ excitation, though this exit channel seems to be very likely, both from the energy-loss spectra, Fig. 1, and from theoretical considerations, cf. Sec. VII D. This apparent discrepancy has the following explanation. The $(^1D)\ 3p^2$ (singlet) level has an energy slightly above the first excited states of Ne^+,[25] and therefore decays preferentially by emission of an electron with very low energy ($\sim\frac{1}{2}$ eV) into, e.g., the excited $(^1D)\ 3s$ Ne II state.[22] This implies a correspondingly strong optical emission of the 407-Å $2p^5\,^2P$-$2p^4(^1D)\ 3s'\,^2D$ Ne II line. The 407-Å line dominates indeed the uv spectrum of the Na^+-Ne collision,[26] as will be discussed further in the section below on the optical spectra.

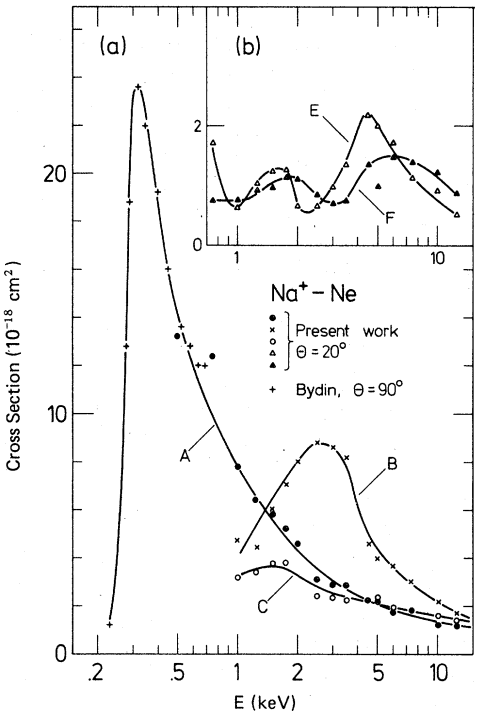

FIG. 10. Cross section for excitation of the lines indicated on Fig. 9, measured at $\theta = 20°$. The low-energy results by Bydin *et al.*, Ref. 21, measured at 90°, are normalized to our results. The cross sections for the two sodium lines E and F show an oscillatory behavior, further analyzed in Fig. 11.

Two of the sodium lines, E and F, show an oscillatory behavior, see the insert in Fig. 10. In Fig. 11 the cross sections are plotted as function of the inverse collision velocity. The extrema are seen to be equally spaced in $1/v$, with the same spacing for the two curves, but different initial phases. Lines E and F correspond to the two processes

$$Na^+ + Ne \rightarrow \begin{cases} Na(2s^2 2p^5 3s3p) + Ne^+ \ \text{(line } E\text{)} \\ Na(2s^2 2p^5 3s3d \text{ or } 3p^2) + Ne^+ \ \text{(line } F\text{)}. \end{cases}$$

Inspection of Table I shows that these exit channels, leading to sodium autoionizing states, have energy defects similar to the exit channels

$$Na^+ - Ne \rightarrow Na^{+}*(3s \text{ or } 3p) + Ne*(3s \text{ or } 3p),$$

leading to optical emission from Ne and Na^+. This opens up the possibility of Rosenthal-type interferences between two or more of these channels. One should accordingly analyze the structure of the emission cross sections from the (24) non-metastable Ne I and Na II $3s$ and $3p$ levels. The emission from the Na II $3s$ and $3p$ levels has never been studied systematically, but Belik *et al.*[26] have investigated one of them, the Na II $2p^6\,{}^1S$-$3s[\frac{3}{2}]^\circ$ transition at 376.2 Å. The emission cross section

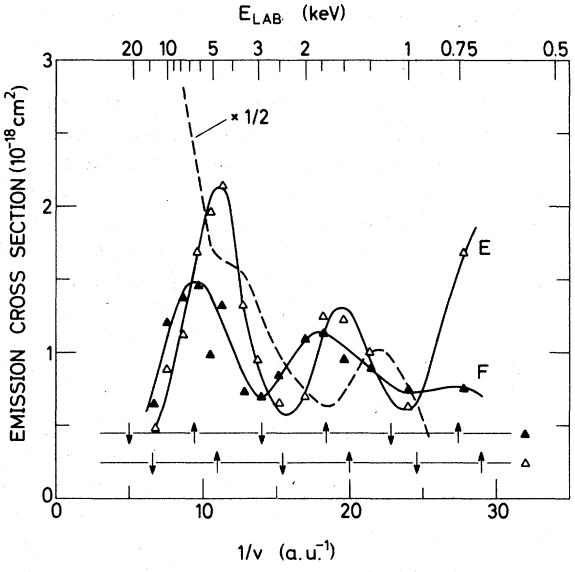

FIG. 11. Oscillatory behavior of the lines E and F, corresponding to the autoionizing sodium levels $2s^2 2p^5 3s3p$ (E) and $2s^2 2p^5 3s3d$ or $3p^2$ (F). The frequencies are the same, but the initial phases are different, as indicated by the arrows. The dashed line shows the emission cross section of the Na II $2p^6\,{}^1S - 3s[\frac{3}{2}]_0$ line at 376.2 Å, taken from Ref. 11, and multiplied by $\frac{1}{2}$. This cross section has a superimposed undulation with comparable amplitude and a period similar to the period for the E and F lines, but about 180° out of phase with F.

of this line is indicated with a dashed curve on Fig. 11, and it is seen also to exhibit a superimposed undulation with comparable amplitude and a period similar to the period for the E and F lines, but about 180° out of phase with F. It is, however, not possible to identify the interfering terms uniquely, since the oscillatory structure of the Na II 376.2-Å line might be partly or entirely due to cascading, probably from the Na II $3p$ levels, in analogy with the observation by Bobashev and Kharchenko,[27] that the two Ne I $3s$ levels are mainly populated by cascades from the ten Ne I $3p$ levels. The search for oscillations in the emission cross sections from the Ne I $3s$ and $3p$ levels, that would correspond to the oscillations seen in Fig. 11 is almost hopeless, because these cross sections are dominated by the well-known Rosenthal oscillations between the one-electron excitation channels $Na(3p) + Ne$ and $Na^+ + Ne(3p)$ observed by Tolk *et al.*[28] and Andersen *et al.*,[9] having considerably larger cross sections. However, in their detailed analysis of this interference Tolk *et al.*[28] calculated the sum of the Na($3p$) and Ne($3p$) cross sections (Fig. 5 of Ref. 28). If the $3p$ levels were populated exclusively by the one-electron excitation channel, as assumed by Tolk *et al.*, one would expect this sum curve to vary smoothly with energy. But above 1 keV weak undulations are actually seen in the sum curve, with similar amplitude, but in almost opposite phase to the E and F curves in Fig. 11. Furthermore, the weak undulations in the sum curve seem to be due to slightly more pronounced oscillations in the Ne($3p$) channel, as compared to the Na($3p$) channel oscillations. We therefore suggest that this additional structure in the sum curve for excitation of a $3p$ electron *is most probably due to a contribution from the two-electron processes discussed above*, a possibility neglected in the model of Tolk *et al.*

V. PHOTON SPECTROSCOPY

The photon spectra from the Na^+-Ne collision have been investigated by several authors,[9,26-29] both in the uv and in the visible range. Inspection of Table I shows that most often the spectral lines can arise from several exit channels, and in many cases both from one- and two-electron excitations. The picture is even further complicated by cascade processes and by the possibility that some ionic levels may be populated by decay of an autoionizing level of the atom, as mentioned in Sec. IV. In this section, results of some measurements will be reported which were performed in order to investigate the plausibility of this latter mechanism. In Sec. VI the relative role of all the different mechanisms leading to photon emission will be discussed.

In the analysis of the autoionization processes it was argued that the (^1D) $3p^2$ autoionizing neon level decays to the excited (^1D) $3s$ Ne II level by emission of a low-energy electron. The uv spectra measured by Belik *et al.*[26] show that the $2p^5\,^2P$-$2p^4(^1D)\,3s'\,^2D$ emission at 407 Å is responsible for about $\frac{2}{3}$ of all emission in the ultraviolet. The remaining part consists of emission lines from Na II, Ne I, and Ne II. It is important to note that the $3s''\,^2S$ and $3s\,^2P$ Ne II levels, for which the core configurations are $2s^2 2p^4\,^1S$ and ^3P, respectively, are seen, but they are considerably weaker than states with a ^1D core. The importance of the various core configurations will be analyzed in Sec. VII D.

The role of cascade contributions to the (^1D) $3s'\,^2D$ level from higher levels has been analyzed. Spectra recorded in the relevant optical range (3000–4000 Å) showed only two Ne II lines with strong intensity, and both of these cascade either directly or indirectly to the $3s'\,^2D$ level. They are the 3571-Å Ne II $3s'\,^2D$-$3p'\,^2F$ transition, and the 3229-Å Ne II transition which is the sum of the $3s'\,^2D$-$3p'\,^2D$ and the $3p'\,^2F$-$3d'\,^2G$ transitions at 3231 and 3227 Å, respectively. Their emission cross sections were measured and the results shown in Figs. 12(a) and 12(b). The absolute values are accurate within 50%. The polarization was small for both lines over the entire range of collision energies studied. Figure 12(c) gives the emission cross section for the 407-Å line here obtained, shown together with the results of Belik *et al.*,[26] who claim an uncertainty of 20% in their absolute values. It should be noted that both cascade contributions to the 407-Å line exhibit an energy dependence different from what is observed for the 407-Å line, particularly in the region 1–2 keV. Taking the magnitude of the cascade into account, it can be concluded that though their contribution to the 407-Å line emission is significant, they cannot be the dominant contributors to the size and shape of this cross section. The left side of Fig. 12 shows in detail the threshold behavior of the three lines. Comparison with Fig. 9 shows that the onset of excitation for the spectral lines takes place in the same energy region as the onset of excitation of the autoionizing states. It therefore seems very likely that at least part of the 407-Å emission is a secondary effect, the primary event being the excitation of a (^1D) $3p^2$ (or higher-lying) autoionizing level.

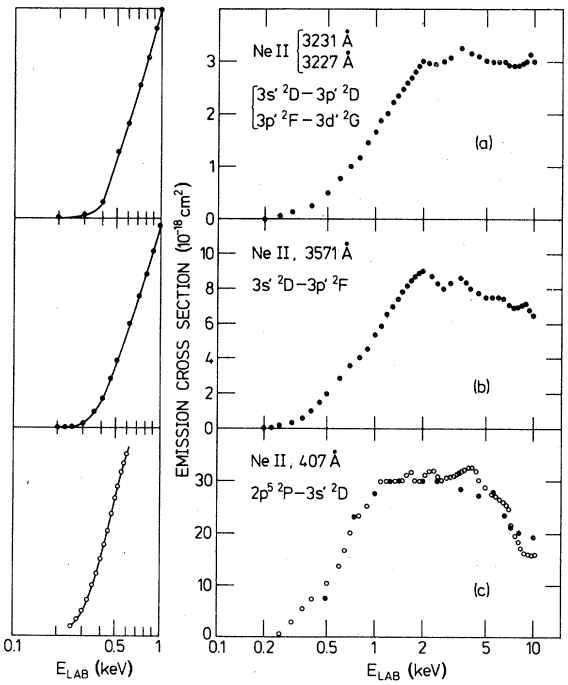

FIG. 12. Emission cross sections of three Ne II lines, all having a (^1D) core. (●) Present results. (○) Belik *et al.*, Ref. 13. These lines are the most prominent Ne II lines observed in the optical spectra for this collision. The lines (a) and (b) cascade directly or indirectly to the line (c). The detailed plots to the left show the threshold behavior in an expanded scale.

VI. RELATIVE IMPORTANCE OF THE EXCITATION PROCESSES

The problem of the relative importance of the various channels leading to photon and electron emission will be discussed here, using Tables I and II as starting points. It should be borne in mind that several channels may contribute to each of the individual optical emission cross sections. As seen from Table II, the relative sizes of the cross sections corresponding to peaks B, C, B', and C' do not change drastically with energy. Consequently the discussion is restricted to the 2-keV data, for which the most detailed information is available. In the discussion the autoionization processes must also be taken into account, since these processes will contribute to peak C. The sum of the cross sections for the discrete lines discussed in Sec. IV amounts to about 1.7×10^{-17} cm^2 at 2 keV. Since Na^+ excitation only takes place in connection with simultaneous excitation of a neon electron, an estimate of the role of this exit channel, which also contributes to peak C, can be obtained from the estimate of Belik *et al.*[26] of 0.8×10^{-17} cm^2 for the emission cross section for the $3s$ Na II multiplet. This cross section will include both direct excitation and cascades from higher levels, among which the $3p$ levels are expected to dominate. Inspection of Table I shows then that the contribution from the Ne I $3s$ and $3p$ excitation, connected with two-electron excitation,

must be of similar magnitude. How this part of the excitation is distributed between $3s$ and $3p$ (or higher excited) electrons cannot be decided from the present set of data. But it is very likely that part of the Ne I $3p$ excitation observed in the experiments of Tolk *et al.*[28] and Andersen *et al.*[9] is due to two-electron processes, as already proposed by the analysis in Sec. V, and that certainly the Ne I $3s$ emissions measured by Bobashev[29] are populated also from these channels.

The importance of these contributions, relative to the one-electron excitations, will now be analyzed. The one-electron capture cross section (peak B') is estimated to be about 4.1×10^{-17} cm^2. It is seen from the TOF spectra, Fig. 2, that the overwhelming part of this process is capture into the Na($3p$) levels. A measurement performed at our laboratory yielded a value of 3.0×10^{-17} cm $\pm30\%$ for the emission cross section of the Na I $3\,^2S$-$3\,^2P$ resonance multiplet. This estimate was obtained by normalization to the known cross section for this transition for the neutral Na-Ne collision,[30] measured with the same apparatus. This suggests that the absolute value claimed by Tolk *et al.* of 1.4×10^{-17} cm^2 for this process at 2 keV is too small by a factor of 2 or 3. Since the relative cross sections of Tolk *et al.* are accurate within 5%, the emission cross section for Ne I $3p$ emission should be increased accordingly, from 0.6 to about 1.8×10^{-17} cm^2. Our value for neon one-electron excitation (peak B) is also 1.8×10^{-17} cm^2. Although minor excitation of the Ne I $3s$ levels cannot be excluded, it follows both from an inspection of Fig. 1(a) and from the analysis of the Ne I $3p\rightarrow3s$ cascades by Bobashev and Kharchenko,[27] that the Ne($3p$) excitation is dominant. It can thus be concluded that most of the light observed from the decay of Na I $3p$ and Ne I $3p$ levels originate from one-electron excitations, but that the *contributions from two-electron excitation could amount to about 20%*. This latter contribution probably explains the discrepancy between experiment[9,28] and the calculations by Nikitin *et al.*[31] In their calculations, based on a one-electron excitation description, Nikitin *et al.* predicted zero intensity from light originating from the Ne I $3p[\frac{5}{2}]_3$ level. Experimentally, however, this level is found to have a small but nonvanishing excitation probability.[28] The level has pure triplet character and would thus not be expected to be populated in a one-electron excitation process if the Wigner spin-conservation rule holds for the Na^+-Ne system. The validity of the Wigner rule for this system is strikingly confirmed by the electron spectra (see Fig. 9 and Ref. 22). Consequently, the conclusion drawn by Tolk *et al.*,[28] that the Ne I $3p$ triplet excitation is due to a large spin-orbit interaction in the $(Na\text{-}Ne)^+$ molecule, causing a breakdown of the Wigner rule, is questionable. Although the algebra and the fitting of the data performed by Tolk *et al.* are correct, their analysis only shows that Ne($3p$) $^3L_{M_L=\pm1}$ states must be formed. However, when simultaneous target excitation occurs, this does not necessarily imply that a triplet molecular state $^3\Lambda$ is populated. The results concerning the relative singlet-triplet contribution to the oscillatory part of the cross section given by Tolk *et al.*[28] (p. 980) actually mean (LSM_LM_S notation)

$$^1L(10\pm10):{}^1L(20\pm10):{}^3L(11\pm11):{}^3L(21\pm11)$$
$$=13:13:6:1.2\,.$$

If, as suggested by the electron spectra, the Wigner rule holds for this system then the Ne ^3L excitation should come from two-electron excited channels implying a simultaneous excitation of Na^+ ^3L states. From the above result of Tolk *et al.* about 22% of Ne ^3L should be formed prior to the final long-range recoupling establishing the ten Ne($3p$) atomic levels. As about 20% of the light from Ne($3p$) excitation originates from two-electron excitation, this means that two-electron processes yield predominantly Ne triplet levels. This will be confirmed by the detailed analysis presented in Sec. VII D below. A direct experimental proof concerning the origin of the triplet excitation will require measurements based on coincidence techniques.

The content of peak C', 3.7×10^{-17} cm^2, suggests that most of the capture connected with two-electron processes leads to the Na($3s$) ground state since the experiments show that most of the Na($3p$) excitation is due to one-electron excitation. Peak C' will simultaneously lead to excitation of Ne II $3s$, $3p$, or higher levels, including ionization giving rise to a free electron in the continuum. This is consistent with the estimated population cross section of the Ne II $3s$ levels, 7.5×10^{-17} cm^2 of Belik *et al.*,[26] leaving ample space for a considerable contribution to this cross section from the expected cascades from the autoionizing neon (^1D) $3p^2$ level mentioned earlier. Many channels in peak C and C' will give rise to electron emission; especially, the large size of peak C, 6.7×10^{-17} cm^2, would suggest an important continuum of free-electron energies. That this continuum is indeed very large is seen from Fig. 9. An estimate of the cross section from an integration of the recorded electron spectra gives a value of about 10×10^{-17} cm^2 at 2 keV, with an uncertainty about 50%, mainly caused by difficulties with precise recording of the low-energy part (<5 eV) of the electron distribution.

So, despite the uncertainty of some of the ab-

solute magnitudes of the cross sections from the different processes, it is possible to obtain a consistent picture of the relative importance of the many groups of different processes listed in Table I. The discussion has also shown that this consistency can only be achieved by combining information from all three kinds of measurements: differential energy loss and time-of-flight, electron spectroscopy, and photon spectroscopy. If information on each specific exit channel in Table I is wanted, coincidence measurements will be required.

VII. MOLECULAR ENERGY DIAGRAM

The goal of this section is the presentation of a molecular energy diagram, Figs. 14–17, for the $(Na\text{-}Ne)^+$ molecular ion, computed theoretically and verified experimentally, with the level crossings accurately located and the couplings between the intersecting states determined. As pointed out in the Introduction, this final molecular diagram is a genuine synthesis of several separate experimental and theoretical efforts. No single effort in isolation could have produced the final level diagram obtained here. For heuristic purposes, however, the analysis of the physical processes will be presented in terms of the calculated molecular energy diagram. It is easier to understand the physics presented in terms of the molecular picture finally obtained, rather than to chronicle the interplay that led up to this result.

To orient the reader, subsection A describes the general features of the MO diagram for the $(Na\text{-}Ne)^+$ system and the couplings leading to one- and two-electron excitations. It relies heavily on the similarities between this system and the symmetric Ne-Ne system. Subsection B describes the molecular calculations, while C and D present the molecular diagram finally obtained and analyze the experimental results in terms of this molecular energy level diagram. Subsection E presents a simplified level scheme with a few adjustable parameters with which the calculated molecular energy diagram can be directly verified by experiment.

A. Analysis of the MO diagram

Starting from the basic one-electron picture, it is well known that the interactions in a system consisting of two L shells are primarily determined by the strong promotion of the $4f\sigma$ orbital. This was pointed out by Lichten[32] for the symmetric Ne-Ne system. Except for minor changes in the u-g character of the orbitals, the slightly asymmetric $(Na\text{-}Ne)^+$ system should be very similar. A *schematic* $(Na\text{-}Ne)^+$ MO diagram is presented

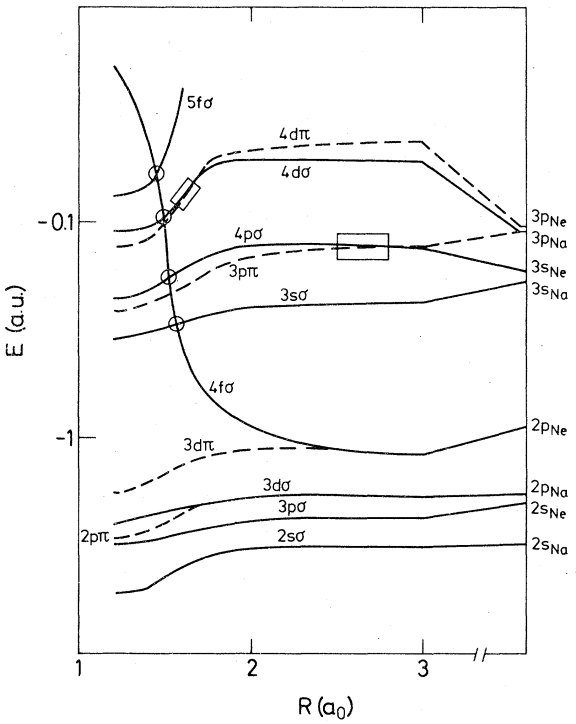

FIG. 13. Schematic diabatic MO correlation diagram for the $(NaNe)^+$ system. The shape of the energy curves and their absolute position are estimated from a compilation of various results of the calculations (Ca1, Ca2, Ca3) described in Sec. VII B.

in Fig. 13. The details of the calculations on which this estimate is constructed will be described in subsection B below. At the crossings of the $4f\sigma\,(\sigma 2p_{Ne})$ orbital with empty Rydberg MO's, *one*- and *two*-electron transitions will give rise to the experimentally observed "triple peak" structure seen in Figs. 1 and 2. From an examination of the simple MO diagram, one expects the inelastic processes to produce the following categories of excited states:

(i) *One-electron excitations*, which can be described schematically as

$$[Na^+(2p^6)+Ne^+(2p^5)]_{\text{core}}+1 \text{ Rydberg electron}\,.$$

Depending onto which core the Rydberg electron will finally be bound, the following two channels will be populated[9,28,29]:

Ne excitation, $Na^+(2p^6)+Ne^*(2p^5nl)$;

electron capture, $Na(2p^6nl)+Ne^+(2p^5)$.

Due to the quasisymmetric character of this system the transition probability is expected to be small at the first $4f\sigma_{(u)}$-$3s\sigma_{(g)}$ crossing. As was the case with the Ne-Ne system,[33] this crossing in Na^+-Ne should lead to Ne(3s) and Na(3s) ex-

citation (quasi u-g resonance electron transfer). However, just as in the Ne-Ne system, the $4p\sigma_{(u)}$-$3p\pi_{(u)}$ rotational coupling will very efficiently transfer the excited electron to the Ne($3p$) and Na($3p$) levels, thereby explaining the observed dominance of $3p$ excitation, Figs. 1 and 2. The role of the other crossings will be discussed in subsections C and D.

(ii) *Two-electron excitations,* which can be described schematically as

$$[Na^+(2p^6)+Ne^{2+}(2p^4)]_{\text{core}}+2 \text{ Rydberg electrons}.$$

Depending onto which core the electrons will finally be bound, the following three channels are expected to be populated

$$Na^+(2p^6)+Ne^{**}(2p^4nln'l'),$$

$$Na^*(2p^6nl)+Ne^{+*}(2p^4n'l'),$$

$$Na^{-*}(2p^6nln'l')+Ne^{2+}(2p^4).$$

Similar arguments as for the one-electron excitation will explain the observed importance of $nln'l'=3s3p$ and $3p^2$ (Figs. 1 and 2). It will be shown in subsection D, however, that core rearrangement processes complicate the pattern.

B. Quasimolecular calculations

In order to obtain the most appropriate descriptions of the various excitation processes, different theoretical approaches have been selected in different ranges of internuclear distance. All calculations start from LCAO-STO-MO expansions (linear combination of atomic orbitals, Slater-type orbitals, molecular orbitals). The STO expansion basis is that previously used by Gauyacq[33] for the Ne_2 system. It has been verified that the Ne basis set is sufficiently large and flexible to enable a correct description of the Na atom in its ground and first excited state. For example, the calculated Na $3s$-$3p$ energy separation amounts to 2.05 eV compared with the experimental value 2.10 eV. In order to get a good description of the incident channel and of the *primary* transitions at the $4f\sigma$-$nl\sigma$ MO crossings, an SCF (self-consistent field) calculation has been carried out on the $X\,^1\Sigma^+$ ground state of $(Na\text{-}Ne)^+$. The description of the diabatic $4f\sigma$-$nl\sigma$ MO crossings has been achieved using the frozen orbital (FO) method introduced by Gauyacq.[33] For this purpose, at $R=2.0$ a.u. the LCAO expansion coefficients of the outer MO's are frozen and subsequently used in the region $1.2<R<2.0$ a.u. In this region of small internuclear distances where the important curve crossings are located, single-configuration states generated by the virtual orbital (VO) method[34] are used to describe *one*-electron excitation channels (A series) and *two*-electron excitation channels (C series). In each series, a limited configuration interaction (CI) is performed to improve the energy of the excited states without losing the diabatic description of the primary crossings. This set of calculations will be referred to as Ca1 and the corresponding potential curves are shown in Fig. 14.

The calculation Ca1 is not *a priori* the most appropriate for the representation of the secondary mechanisms occuring between excited states. For example, the study of the $2p_{Na}-2p_{Ne}$ core sharing (see Sec. VII D), requires a correct description of the $Na^+(2p^6)$ and $Ne^+(2p^5)$ core configuration. This aim is achieved with an SCF calculation on a singly excited state of $(Na\text{-}Ne)^+$: in practice the lowest $^3\Sigma^+$ excited state has been chosen (calculation Ca2). In the same spirit, the representation of the doubly excited states (see Sec. VII D) has been obtained, using an SCF calculation on the excited $(Na\text{-}Ne)^{2+}$ $^4\Delta$ molecular state dissociating into $Na^+(2p^53s)+Ne^+(2p^5)$ (calculation Ca3). The calculations have been carried out using the ALCHEMY program of Bagus *et al.*[35] In Fig. 14 and Table III the ground-state potentials obtained in the Ca1 and Ca2 calculations are compared with

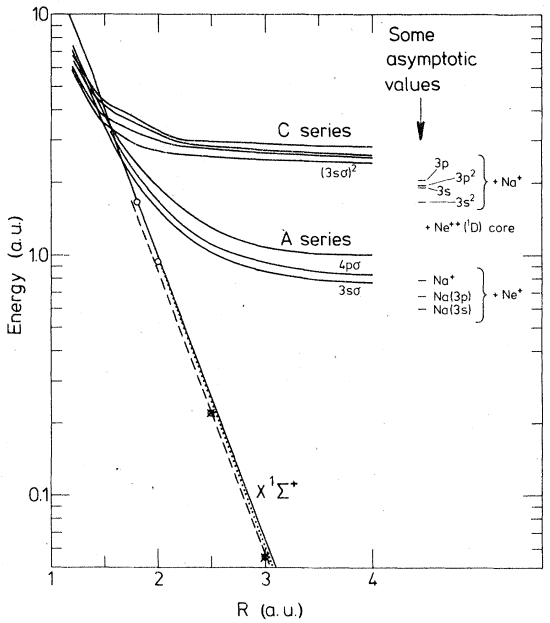

FIG. 14. Some $^1\Sigma^+$ potential-energy curves of the $(NaNe)^+$ system: (—) from calculation Ca1 involving an SCF calculation on the $(NaNe)^+$ $X\,^1\Sigma^+$ ground state, the frozen orbital method for $R\leq 2a_0$ and a partial diagonalization in each of the A and C series. (○) from calculation Ca2 based on an SCF calculation on the lowest $(NaNe)^{+*}$ $^3\Sigma^+$ excited state; (---) the experimentally derived potential of Kita *et al.* (Ref. 19); (×) analytical potential of Efremenkova *et al.* (Ref. 36) based on an asymptotic theory for interatomic interactions; (····) analytical potential of Sondergaard and Mason (Ref. 37) based on scaling laws for closed shell interactions.

TABLE III. Comparison between different predictions for the $X^1\Sigma^+$ ground-state potential energy curve of the (Na-Ne$^+$ system. The energies and R are given in a.u. The depth and position of the well at large distances in the $X\,^1\Sigma^+$ curve of $(NaNe)^+$ given in the paper of Efremenkova *et al.* (Ref. 36) are not consistent with the analytical expression for the repulsive part of the potential. Their results can be fitted by using a constant preexponential factor in their formula, giving $V(R) = 70R^{2.4132}\exp(-3.124R) - 1.33/R^4$, see Masnou-Seeuws *et al.* Ref. 36.

R	Kita *et al.* Ref. 19	Sondergaard and Mason Ref. 37	Kim and Gordon [a]	Efremenkova *et al.* Ref. 36	Present Ca1 FO	Present Ca1 SCF	Present Ca2
1.2	7.61	8.800			9.065	5.816	
1.4	4.43	5.077			5.391	3.713	
1.5	3.38	3.857			4.115	3.349	3.519
1.6	2.57	2.929			2.959	2.769	
1.8	1.50	1.690			1.687	1.667	1.639
2.0	0.87	0.975			0.982		0.950
2.5	0.225	0.246	0.231	0.225	0.258		0.242
3.0	0.058	0.062	0.060	0.068	0.065		0.055
4.0	0.0038	0.004	0.0032	0.0022	0.0008		0.002

[a] Y. S. Kim and R. G. Gordon, J. Chem Phys. 60, 4323 (1974).

the experimentally derived potential by Kita *et al.*,[19] and the analytical potential proposed by Efremenkova *et al.*[36] There is good agreement among all these four ground-state potentials. There is also seen to be good agreement with the potential derived from the scaling laws of closed-shell interactions, as described by Sondergaard and Mason.[37] This justifies the use of the potential of Kita *et al.*,[19] used for the normalization of the experimental data (Sec. III B), and for the scattering calculations below (Sec. VII E).

C. One-electron transitions

1. Excitation of the n=3 levels of Na and Ne

The significant states of the A series derived from the Ca1 calculations for the range of internuclear distances $1.2 \leq R \leq 10a_0$ are plotted in Fig. 15. For $R > 10$, the $\pi 3p_{Na} - \pi 3p_{Ne}$ energy splitting $\Delta U(R)$, which will be relevant in the following discussion has been extrapolated using the Smirnov[38] asymptotic theory for charge exchange. Explicitly $\Delta U(R)$ is obtained from the formula

$$\Delta U(R) = [\Delta E_\infty + \Delta(R)]^{1/2}, \tag{1}$$

where

$$\Delta(R) = A\exp(-\alpha R)R^\beta \tag{2}$$

with $A = 0.0189$ a.u., $\alpha = 0.4688a_0^{-1}$, $\beta = 2.2669$, and $\Delta E_\infty = 4.8\times10^{-3}$ a.u.[39] At the two first crossings (A_1, A_2) with the incident $X\,^1\Sigma^+$ channel at $R \simeq 1.65a_0$ the $3s$ channel is populated (the expected $3s$ excitation threshold is given in Table IV). Following that, the corresponding probability amplitudes coherently mix, as described by Tolk *et al.*,[28] to give interference patterns in the total $3s$ excitation cross sections. The location ($R \simeq 13a_0$) of this secondary coupling region has been estimated according to the Smirnov[38] and Demkov[40] theories. The characteristic area between the energy curves that governs the oscillation frequency[41] thus amounts to $\langle ER\rangle \simeq 0.86$ a.u.

As already found in the comparison of the Li^+-He quasisymmetric system with He-He,[42] it is also found here that the interaction ($H_{A_1} = 0.04$ a.u.) at the quasi u-g (A_1) crossing is smaller than that of the quasi u-u (A_2) crossing ($H_{A_2} \simeq 0.1$ a.u.). It is thus expected that the dominant primary transition occurs at A_2. However, as indicated in Fig. 15, the $4p\sigma$ state is likely to interact via rotational coupling with the $3p\pi$ state in the range $2a_0 \lesssim R \lesssim 4a_0$. The very same situation has been found and discussed by Gauyacq[33] for the isoelectronic symmetric system $(Ne)_2$. It can therefore be inferred that the $4p\sigma$ state will be strongly depopulated, leading to dominant excitation of the $3p$ channels in agreement with experiment. The $3p$ excitation threshold is thus determined by the potential energy at the A_2 crossing, Table IV.

The population of only the $3p\pi$ channel cannot account for the Rosenthal[41] oscillations in the $3p_{Na}$ and $3p_{Ne}$ total cross sections reported by Tolk *et al.*[28] This effect requires the simultaneous population of both the $3p\pi$ and $4d\pi$ channels. It is readily seen from Fig. 15, that a similar situation as that discussed for the $4p\sigma$-$3p\pi$ transfer, also occurs for the $4d\sigma$-$4d\pi$ channels. Indeed the $4d\sigma$ state which is initially populated at the A_3 crossings transfers most of this population to the $4d\pi$ channel. This rotational coupling is expected to be efficient, since it involves two Rydberg orbitals having the same orbital angular momentum ($l = 2$).

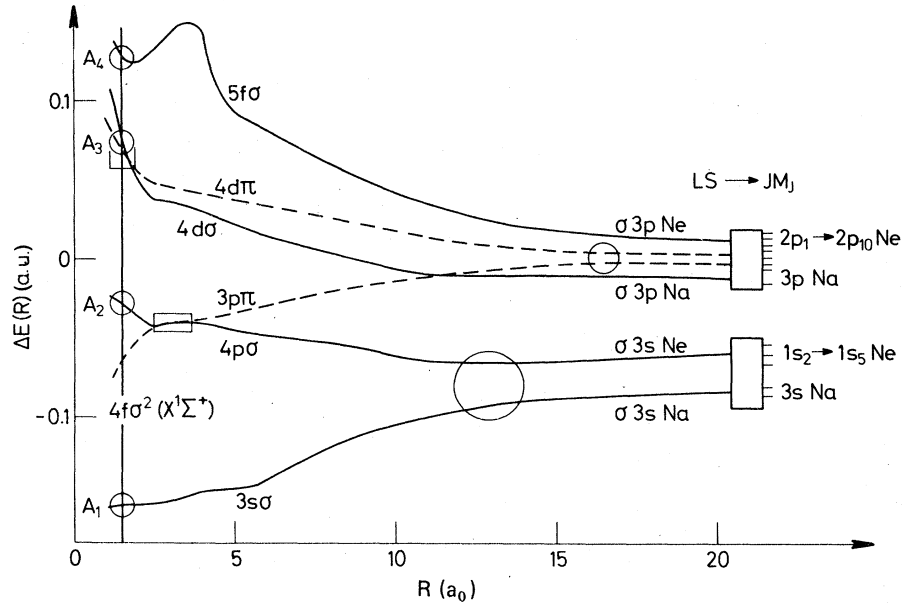

FIG. 15. Detailed view of energy curves of the A series correlated with Na or Ne $n=3$ levels, relevant for the discussion of the one-electron transitions. The curves are referred to the mean value of the shown $^1\Pi$ energy curves. For $R>10a_0$ the curves are analytically extrapolated using the Smirnov asymptotic theory (Ref. 37). For convenience the states have the same labels as their characteristic Rydberg MO's [i.e., $nl\sigma \equiv (\cdots 4f\sigma nl\sigma)$]. The small circles locate the primary transition via radial coupling from the incident state. The squares locate the rotational electron transfer. The circles at large R indicate the outer sharing via quasiresonant charge exchange.

This very argument is that which rules out the simpler mechanisms involving direct $4f\sigma$-$3p\pi$ and $4f\sigma$-$4d\pi$ rotational couplings.[33,43] In summary, in a first step the $4p\sigma$ and $4d\sigma$ orbitals are populated via *radial* coupling; almost simultaneously these populations are transferred to their "mate" π orbitals under the action of the rapid rotation of the internuclear axis. As discussed above for the $3s_{Na}$-$3s_{Ne}$ population sharing, the probability amplitudes are then mixed giving rise to oscillations in phase opposition in the Na($3p$), Ne($3p$) total excitation cross sections.[28] The location of the $\pi 3p_{Na}$-$\pi 3p_{Ne}$ transition region $R_{C\pi}=16.5a_0$ is obtained from the relation $\Delta(R_{C\pi})=E_\infty$ [see Eq. (2)]. The characteristic area between the $4d\pi$ and $3p\pi$ states for $1.6a_0 \lesssim R \lesssim 16.5a_0$ derived from the curves of Fig. 15 amounts to $\langle ER\rangle \simeq 0.65$ a.u. This value is in reasonable agreement with $\langle ER\rangle = 0.883$ a.u. as obtained from the experimental data.[28] It can be noticed that the A_3 crossing again presents a quasi u-g character leading to a smaller interaction (0.03 a.u.) than that at the A_2 crossing. The $4d\pi$ state is thus expected to have a much weaker population than that of the $3p\pi$ state. This expectation is supported by analysis of the Rosenthal oscillations in the Na($3p$) and Ne($3p$) cross sections (Fig. 4 of Ref. 28). The transition probability at A_2 is about a hundred times larger than at A_3. (It can be easily shown that such a small relative population of the $4d\pi$ channel still conveys large oscillations). The experimental ratio $R=P_{Ne}/P_{Na}$ of the direct to the exchange $3p$ excitation deduced from analysis of the results of Tolk *et al.*[28] is $R=0.58$ at $E=1$ keV and $R=0.62$ at

TABLE IV. Na^+-Ne excitation threshold energies (c.m.), in eV.

	Theory	Expt.	Expt. channel
$1e^-$ processes	$R_{X,A_1}\sim 68$	~75 [a]	Ne($3s$)
	$R_{X,A_2}\sim 71$	~120 [b]	Na, Ne($3p$)
Ne ionization	•••	~81 [c]	•••
$2e^-$ processes	$R_{X,C}\sim 88$	~107 [d]	Ne(^1D)$3s^2$
	$R_{A,C}\sim 95$	≤107 [e]	Ne(^1D)$3s^2$
		~107 [f]	Ne^+(^1D)$3s$
		~85 [g]	Ne(^1D)$3s^2$

[a] S. V. Bobashev, Ref. 29 (estimate based on his figure).
[b] N. H. Tolk *et al.*, Ref. 28.
[c] O. Beeck and C. Mouzon, Ann. Phys. 11, 858 (1931).
[d] V. I. Ogurtsov and Yu. F. Bydin, Zh. Eksp. Teor. Fiz. 57, 1908 (1969). [Sov. Phys. JETP 30, 1032].
[e] Yu. F. Bydin *et al.*, Ref. 21.
[f] V. P. Belik *et al.*, Ref. 26.
[g] Yu. F. Bydin and S. S. Godakov, Pis'ma Zh. Eksp. Teor. Fiz. 23, 566 (1976) [JETP Lett. 23, 518 (1976)].

3 keV. The present experiment (see Table II) yields $R = 0.45$ at 1 keV, in good agreement with theoretical estimates based on the Demkov-Meyerhof formula: $R = 0.43$ at 1 keV and $R = 0.61$ at 3 keV. The Demkov-Mayerhof formula is, with v and I in atomic units[40,44]

$$R = \exp\{-(\pi\sqrt{2}/v)[|(I_{Na})^{1/2} - (I_{Ne})^{1/2}|]\}. \quad (3)$$

Finally, the $3p$ excitation can also occur through the population of $^1\Sigma^+$ states[33] (namely, $4d\sigma$ and $5f\sigma$, see Fig. 15). In particular, the interaction at A_4 is sufficiently large (0.07 a.u.) to induce a significant population of the $5f\sigma$ state.

2. *Absence of Na^+ excitation: Comparison with K^+-Ar*

It was pointed out in Sec. III A that no excitation of the sodium ion was observed without simultaneous excitation of neon. The importance of various mechanisms for single Na^+ excitation is analyzed below, and a comparison is made with the superficially similar K^+-Ar system, for which excitation of K^+ states without simultaneous Ar excitation is significant.

Inspection of the $(Na\text{-}Ne)^+$ MO diagram (Fig. 13) shows that single Na^+ excitation would involve a one-electron excitation ($4f\sigma \rightarrow nl\sigma$) with a subsequent transfer, during the separation, of the $4f\sigma(\sigma 2p_{Ne})$ vacancy to the $3d\sigma(\sigma 2p_{Na})$ orbital. This corerearrangement can be written as

$$[Na^+(2p^6) + Ne^+(2p^5)]_{core} + \text{Rydberg electron}$$

$$\rightarrow [Na^{2+}(2p^5) + Ne(2p^6)]_{core} + \text{Rydberg electron}$$

$$\rightarrow Na^{+*}(2p^5 nl) + Ne(2p^6).$$

The corresponding Rydberg series (B) calculated in the virtual orbital approximation using calculation Ca2 is shown in Fig. 16. The two most obvious mechanisms for this process are: (i) the direct $\sigma_{2p_{Ne}}$-$\sigma_{2p_{Na}}$ transition induced by exchange forces, which may be treated within the Demkov-Meyerhof model.[40,44] The $2p$ vacancy sharing ratio R_1 is given by Eq. (3) where the relevant effective ionization potentials are estimated to be $I_{Na} \simeq 38$ eV and $I_{Ne} \simeq 18$ eV. These effective ionization potentials correspond to the ionization of the considered $2p$ shells, screened by a $3s$ electron. In the 1–10 keV range R_1 varies from 10^{-16} to 10^{-6}, showing that this mechanism is not at all efficient. (ii) A two-electron transition, induced by electron correlation at the crossing of the B and C series, see Fig. 16; the transition probability here has been estimated by the Landau-Zener formula

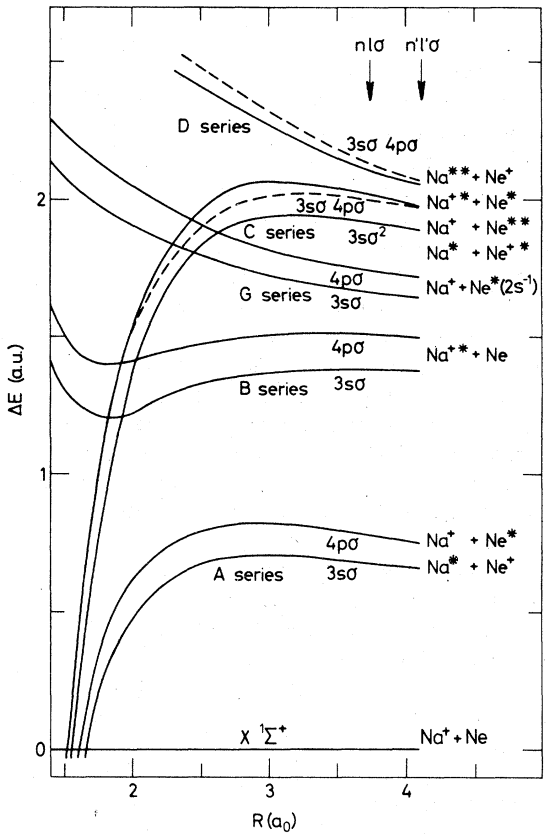

FIG. 16. Some $^1\Sigma^+$ potential energy curves of the $(NaNe)^+$ system referred to the incident diabatic $X\,^1\Sigma^+$ energy curve. This figure shows in addition to the A series (already shown in detail in Fig. 15), the B series corresponding to the molecular configurations $(\cdots 3p\sigma^2 2p\pi^4 3d\sigma 3d\pi^4 4f\sigma^2 nl\sigma)$, relevant to the discussion on the single excitation of Na^+, the G series $(\cdots 3p\sigma 3p\pi^4 3d\sigma^2 3d\pi^4 4f\sigma^2 nl\sigma)$ relevant to the discussion on the absence of $2s_{Ne}$ vacancy production, the C $(\cdots 3p\sigma^2 2p\pi^4 3d\sigma^2 3d\pi^4 nl\sigma n'l'\sigma)$ and D $(\cdots 3p\sigma^2 2p\pi^4 3d\sigma 3d\pi^4 4f\sigma nl\sigma n'l'\sigma)$ series relevant to the discussion on the L-vacancy sharing. The result of a 2×2 diagonalization in the C-D $(3s\sigma 4p\sigma)$ subspace is shown as dashed lines.

$$p = 1 - \exp(-2\pi H_{BC}^2/v\Delta p). \quad (4)$$

Typical values of Δp, the difference in slope at B-C crossings, and H_{BC}, the coupling matrix element, are $\Delta p \simeq 1.1$ a.u. and $H_{BC} \simeq 0.015$ a.u., yielding $p \simeq 2\%$ at 2 keV. Though more efficient than mechanism (i) this transition probability is still too small to lead to a detectable peak in the energy-loss spectrum (Figs. 1 and 2). In the K^+-Ar collision significant one-electron excitation of the K^+ ion has been observed[15,17] in the 1–4 keV region. For this collision mechanism (i) is also completely inefficient ($R_1 \simeq 10^{-11}$ at 1.5 keV), whereas it seems more plausible that mechanism (ii) is more effective for the K^+-Ar system.[45]

D. Two-electron transition

The details of the doubly excited molecular states are shown in Fig. 16. The electron jumps at the crossing between the incident $4f\sigma$ MO and empty Rydberg orbitals (Fig. 13) will give rise to doubly excited molecular states (C series). This generates a triple crossing pattern between the incident $X^1\Sigma^+$ state and the A and C series which is seen in Fig. 14. It is readily seen that the C series can be populated either directly at the $R_{X,C}$ crossings ($1.48a_0 < R_{X,C} < 1.58a_0$) or by a two-step mechanism at the $R_{X,A}$ then $R_{A,C}$ crossings ($1.4a_0 < R_{A,C} < 1.5a_0$). Actually the direct transition, which involves a simultaneous two-electron transition (electron correlation) is expected to be much weaker than the two-step one-electron transition. Inspection of the interaction values at the curve crossings indeed shows that $H_{X,C}$(0.001 a.u.) is much smaller than $H_{X,A}$ and $H_{A,C}$ (0.04–0.1 a.u.). This allows the neglect of the direct X-C transition as is done in Sec. VII E. The theoretical prediction of the threshold for the two-electron excitation total cross sections given in Table IV is seen to be in reasonable agreement with experiment.

The study of the population of the various two-electron excitation channels through the C series is by far more complicated than in the case of one-electron excitations. However, physical insight suggests that the analysis can be reduced to separate investigations of a few simpler mechanisms:

1. Core rearrangement: L vacancy-sharing

The two vacancies created in the $4f\sigma$ MO subsequent to the X-A-C electron transition lead to a $(NaNe)^{3+}$ core which can dissociate in several ways:

type a: $NaNe^{3+} \rightarrow Na^+(2p^6) + Ne^{2+}(2p^4)$;

or

type b: $Na^{2+}(2p^5) + Ne^+(2p^5)$;

or

type c: $Na^{3+}(2p^4) + Ne(2p^6)$.

The two very diffuse Rydberg electrons are assumed to play the role of spectators during the core-dissociation process. The calculation of the relative probabilities of the above three core channels can be reduced to a two-channel charge exchange problem, since the energy levels corresponding to the c products lie far above those of the a and b final states. Depending on the final distribution of the Rydberg electrons between the a and b core types, the following four final channels should be considered: for the a core type,

$Na^*(2p^6nl) + Ne^{+*}(2p^4n'l')$, channel a_1

$Na^+(2p^6) + Ne^{**}(2p^4nln'l')$; channel a_2

the b core type,

$Na^{+*}(2p^5nl) + Ne^*(2p^5n'l')$, channel b_1

$Na^{**}(2p^5nln'l') + Ne^+(2p^5)$, channel b_2.

Figure 16 shows some molecular states corresponding to the a core (C series) and b core (D series). It is seen from Table I that the energy splitting between the a and b core states associated with the same distribution of the Rydberg electrons is approximately equal to 2.5 eV. This strong reduction of the $2p_{Na}$-$2p_{Ne}$ energy splitting as compared to the corresponding value for a single $4f\sigma$ vacancy (Sec. VII C) is obviously due to the *core relaxation* following the double $4f\sigma$ vacancy creation. This effect has already been pointed out for K-vacancy sharing of Li^+-He collisions.[42,46]

The importance of the L-vacancy sharing can be estimated from the Demkov-Meyerhof formula [Eq. (3)] using the "effective ionization potentials" of the $2p$ shells: $I_{Ne} = 29$ eV, $I_{Na} = 30.6$ eV which are the binding energies of $2p_{Ne}$ and $2p_{Na}$ in the $Ne(2p^4\,{}^1D\,3s^2)$ $Na(2p^5 3s^2)$ configurations, respectively. At 6 keV, the sharing ratio $R_2 = p_{Na}/p_{Ne} = 0.30$ thus obtained slightly underestimates the experimental value (0.40) deduced from Fig. 9. A similar estimate for the Ne $2p^4(^1D)3s3p(^1P)$ – Na $2p^5 3s3p\,{}^1P$ L-vacancy sharing yields a ratio $R_2' = p_{Na}'/p_{Ne}' \simeq 0.20$ which again underestimates the experimental value (0.48). This discrepancy can originate from several causes, for example, the neglect of the outer sharing (see subsection D3 below), or different angular distributions of ejected electrons from target and projectile, which may be strongly anisotropic.[22]

2. Core rearrangement: $(2p_{Ne}{}^4)$ $^1D, {}^1S, {}^3P$ core sharing

The two-electron transition at the inner X-A-C triple crossing leaves the core in a $(2p\pi^4 3d\sigma^2 3d\pi^4)^1\Sigma^+$ configuration. The $3d\sigma$-$4f\sigma$ transition has already been investigated above. Thus only type a corresponding to the $[Na^+(2p^6) + Ne^{2+}(2p)^4]$ core need to be considered here. The three possible core states for the $2p^4$ configuration are ^3P, ^1D, and ^1S. However, the feeding channels (C series), having the $(\cdots 3d\pi^4)$ core, correlate at large distance with the $(\cdots \pi 2p_{Ne}{}^4)$ core yielding only the singlet core states. This readily provides the interpretation for the dominance of the ^1D core for both $Ne^{**}(2p^4nln'l')$ autionizing states and $Ne^{+*}(2p^4nl)$ excited states.

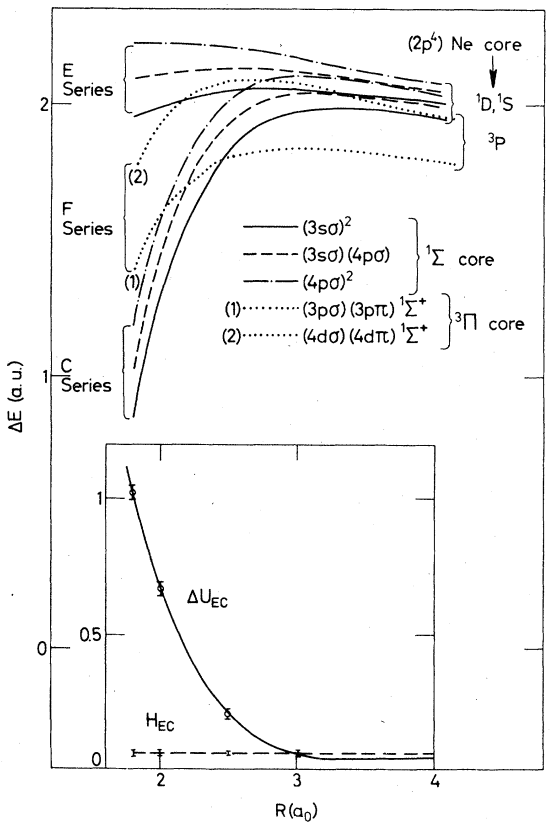

FIG. 17. Some $^1\Sigma^+$ potential energy curves of the $(NaNe)^+$ system (referred to the incident diabatic $X^1\Sigma^+$ energy curve) relevant to the discussion of the $(2p_{Ne}^4)^1D$, ^1S, $3p$ core sharing. In addition to the C series (defined in Fig. 16) are shown in the $E(\cdots 3p\sigma^2\, 2p\pi^4\, 3d\sigma^2\, 3d\pi^2\, 4f\sigma^2 nl\sigma n'l'\sigma)$ and $F(\cdots 3p\sigma^2 2p\pi^4 3d\sigma^2 3d\pi^3 4f\sigma)^3\Pi$ $(nl\sigma n'l'\pi)^3\Pi$ series. In the inset the common energy splitting H_{EC} and interaction ΔU_{EC} between states of the C and E series involving the same two Rydberg orbitals $(nl\sigma n'l'\sigma)$ are shown. The bars indicate the bounds of the variation of the energy splitting for the different pairs of $(nl\sigma n'l'\sigma)$ orbitals.

The possible population of the $Ne^{++}(2p^4\,^3P)$ core states will be discussed later on.

The proper description of $(2p_{Ne}^4)^1D$ and ^1S atomic core states involves both the $(\pi 2p_{Ne}^4)^1\Sigma^+$ and $(\pi 2p_{Ne}^2\sigma 2p_{Ne}^2)^1\Sigma^+$ molecular core states with amplitudes given by

$$\begin{bmatrix} 3d\pi^4 \\ 3d\pi^2 4f\sigma^2 \end{bmatrix} \xrightarrow[R\to\infty]{} \begin{bmatrix} \pi 2p_{Ne}^4 \\ \pi 2p_{Ne}^2 \sigma 2p_{Ne}^2 \end{bmatrix} = \begin{bmatrix} \sqrt{2}/\sqrt{3} & 1/\sqrt{3} \\ -1/\sqrt{3} & \sqrt{2}/\sqrt{3} \end{bmatrix} \begin{bmatrix} {}^1D \\ {}^1S \end{bmatrix}.$$

In Fig. 17 are shown some of the $(\cdots 3d\pi^4 nln'l')$ and $(\cdots 3d\pi^2 4f\sigma^2 nln'l')$ energy levels, the C and E series, respectively. It is seen that the energy splitting $\Delta U_{EC}(R)$ and the electronic interaction H_{EC} between two terms of the C and E series having the same configuration of the Rydberg electrons $(nln'l')$ is to a good approximation independent of $(nln'l')$. The population sharing between the C and E series depends on $\Delta U_{EC}(R)$, $H_{EC}(R)$ and on the collision velocity. However, the C and E series still interact as $R\to\infty[H_{EC}(R\to\infty)\neq 0]$. In order to get rid of this undesirable feature a 2×2 CI has been performed in each $(E, C)_{nln'l'}$ subspace. The matrix elements for dynamical coupling between the resulting $\mathcal{E}$ and $\mathcal{C}$ states are

$$v\left\langle \mathcal{E}\left|\frac{\partial}{\partial R}\right|\mathcal{C}\right\rangle = v\left(H_{EC}\frac{d(\Delta U_{EC})}{dR} - \Delta U_{EC}\frac{dH_{EC}}{dR}\right) \times (\Delta U_{EC}^2 + 4H_{EC}^2)^{-1/2}.$$

A transition between $\mathcal{E}$ and $\mathcal{C}$ will occur when the radial coupling matrix element becomes comparable with the $\mathcal{E}$-$\mathcal{C}$ energy splitting. Inasmuch as the largest value of the $\langle \mathcal{E}\,|d/dR|\,\mathcal{C}\rangle$ matrix element amounts to $0.8a_0^{-1}$ (at $R\simeq 2.5a_0$), it is readily seen that no significant sharing between $\mathcal{E}$ and $\mathcal{C}$ will occur unless the collision energy is greater than about 70 keV. This value is well above the present experimental collision energy range. Consequently, only the states correlated adiabatically with the C series, i.e., the $2p^4\,^1D$ core state are actually populated. This explains the negligible population of the $(2p_{Ne}^4\,^1S)$ core-states.

Among the $(2p_{Ne}^4\,^3P)$ core states, only those issuing from a molecular state having a total singlet electronic spin can be excited according to the Wigner spin-conservation rule. In particular only the $[(2p^4\,^3P)nln'l']^1L$ autoionizing states are expected and indeed seen experimentally. However, the population of such states from the feeding C series requires two-electron rearrangements involving "core Rydberg" electron exchange. In the following typical example

$$(\{\cdots 3d\pi^4\}^1\Sigma^+, \{nl\sigma n'l'\sigma\}^1\Sigma^+)^1\Sigma^+ \quad (C \text{ series}),$$

$$(\{\cdots 3d\pi^3 4f\sigma\}^3\Pi, \{n''l''\pi n'l'\sigma\}^3\Pi)^1\Sigma^+ \quad (F \text{ series}),$$

the C-F transition is induced by intershell electron correlation e.g.,

$$\langle 3d\pi^*(1) n''l''\pi(1)\,|\,1/r_{12}\,|\,nl\sigma^*(2) 4f\sigma(2)\rangle.$$

Since the F series involves a core excited configuration it is expected to be more repulsive than the C series, thus providing F-C curve crossings. The interactions at these curve crossings, which involve Rydberg-core overlaps are expected to be very small. In turn the population

of the $Ne(2p^4\,^3P)$ core states should be weak as is indeed observed in the experimental data (Fig. 9). Singlet states of the F series are plotted in Fig. 17 along with some states of the C series. These states are obtained from the Ca3 calculations. This figure shows that F-C crossings occur in the range of internuclear distances $2a_0 < R < 4a_0$. Actually, for the crossings occurring in the range $2a_0 < R < 3a_0$, the F-C slope differences are large and the transition probabilities estimated by the Landau-Zener (LZ) model are found to be negligible. For high-lying F states, the crossings move outward to the region $3a_0 < R < 4a_0$ and the corresponding F-C slope difference are significantly reduced. Together, these two factors lead to an important enhancement of the transition probability.

It should be stressed that only a few F-C couplings are really efficient in populating the ^3P core states. As an example, a probability of 2% is found for the transition from the $^1\Sigma^+$ molecular state of the C series correlated with $Na(2p^6 3s) + Ne^+(2p^4(^1D)3s)$ to the $^1\Sigma^+$ molecular state of the F series correlated with $Na^+(2p^6) + Ne^{**}(2p^4(^3P)3p^2)$. From Figs. 9 and 10 related to the ejected electrons, the cross section corresponding to the $Ne(2p^4(^3P)3p^2)$ peak, representative of the above mentioned F channel amounts to about 2×10^{-19} cm^2. This gives a cross-section estimate of 10^{-17} cm^2 for the corresponding C channel contributing to the Ne II $2p^5\,^2P$-$3s'\,^2D$ emission. Inspection of Fig. 12(c) shows that this is not unreasonable. It should also be noticed that the LZ formula predicts a decrease of the ^3P core cross sections with increasing energy, as actually observed in the experiments (Sec. IV A).

Finally a few words must be said on the absence of $Ne^*(2s2p^6nl)$ autoionizing states the energy levels of which lie in the neighborhood of the $Ne^{**}2p^4(^3P)nln'l')$ doubly excited states. The vacancy in the $\sigma 2s_{Ne}$ inner orbital is responsible for the repulsive behavior of the corresponding core excited G series (Fig. 16). Transitions at the C-G curve crossings should be the most obvious candidates for populating the $Ne^*(2s2p^6nl)$ states. Since two-electron exchanges between core and Rydberg shells are involved, the interaction at the C-G crossings is expected to be weak. This, together with the large C-G slope differences around $R \simeq 2.5a_0$ (Fig. 16) would yield a very small C-G transition probability. Unfortunately from the computational point of view the correct description of the C-G interactions using a single set of SCF-MO is a very difficult task, since one cannot simultaneously account for the core-relaxation effects in both the initial and final channels.

3. Sharing of Rydberg electrons

After the core rearrangement has taken place in the range $R < 3.5a_0$, the two outer electrons are shared between the two centers of much larger internuclear distances. As already discussed in Sec. VII B, this sharing proceeds along the general lines of near-resonant charge-exchange theory. However, in the present case the number of interacting levels some of which are nearly resonant increases drastically. This suggests that an important sharing via charge exchange will occur between the four main channels a_1, b_1, a_2, b_2, (see subsection D1). However, the problem is still too difficult to be analyzed in detail even with the reduced number of channels. Among these sharing processes a crucial one concerns the possibility of populating the $Ne^*(2p^5 3p)$ triplet states, in connection with the discussion of Sec. VI. In the light of the present theoretical framework and in analogy with the theoretical analysis of the isoelectronic Ne-Ne system,[33] it can be estimated that in most of the energy range the relative population of the dominant doubly excited states is roughly ~30% for the "$3s3p$" excitation, ~60% for the "$3p^2$" excitation, and only a few percent for the "$3s^2$" excitation. The clear evidence of the strong core sharing yielding the $Na^{**}(3s3p)$ autoionizing level (which has already served as a check of the core sharing model presented above) can also be used to demonstrate an important mechanism for populating the $Ne(2p^5 3p)$ triplet states. For this particular case, the various steps leading to $Ne(2p^5 3p)$ triplet excitation by two-electron excitation and population sharing can be schematized in four steps (a)–(d):

$$Na^+(2p^6) + Ne(2p^6) \rightarrow (3d\sigma)^2(4f\sigma)^2$$
$$\rightarrow (3d\sigma)^2(4p\sigma)^2 \quad \text{primary mechanism step (a)}$$
$$\rightarrow (3d\sigma)^2(4p\sigma)(3p\pi) \quad \text{rotational transfer step (b)}$$
$$\rightarrow (\sigma 2p_{Na}\sigma 2p_{Ne})^1\Sigma^+(4p\sigma)(3p\pi)^1\Pi \quad L\text{-vacancy sharing step (c)}.$$

In step (d) the two Rydberg electrons may be shared in four different ways:

$$\rightarrow (Na^{2+} + Ne^+)^1\Sigma^+ + \begin{cases} \sigma 3s_{Na}\pi 3p_{Na} & \text{step (d1)} \\ \sigma 3s_{Ne}\pi 3p_{Na} & \text{step (d2)} \\ \sigma 3s_{Na}\pi 3p_{Ne} & \text{step (d3)} \\ \sigma 3s_{Ne}\pi 3p_{Ne} & \text{step (d4)}. \end{cases}$$

The two configurations relevant for the present discussion are (d1) and (d3). Step (d1) leads unambiguously[47] to

$$Na^{**}(2p^5 3s 3p)^2P + Ne^{+}(2p^5)^2P \quad (\Delta E \simeq 51.35 \text{ eV}),$$

whereas step (d3) leads to a mixture of the following atomic states:

$$Na^{+}(2p^5 3s)^1P + Ne(2p^5 3p)^1L \quad (51.96 < \Delta E < 52.28 \text{ eV}),$$

$$Na^{+}(2p^5 3s)^3P + Ne(2p^5 3p)^3L \quad (51.22 < \Delta E < 51.73 \text{ eV}).$$

It is readily seen that the population of $Ne(2p^5 3p)^3L$ is strongly favored by the quasiresonant outer sharing process. Since decay of the $Na^{**}(2p^5 3s 3p)$ level is one of the dominant lines in the ejected electron spectrum and has an average cross section of 10^{-18} cm^2, the same order of magnitude is expected for the $Ne(2p^5 3p)$ triplet cross section. This is consistent with the amount of $Ne(3p)$ triplet excitation deduced by Tolk *et al.*[28] from the analysis of their experimental data.

It is also worth noting that the observed oscillations (Fig. 11) in the $Na^{*}(2p^5 3s\,3p)$ and in the $Na^{+*}(2p^5 3s)$ cross sections is a further confirmation of the outer sharing description discussed above. The oscillations in triplet state cross sections observed by Tolk *et al.* should, of course, have the same origin. Comparison of the oscillation period in Fig. 11 and in the data of Tolk *et al.* shows that it is almost the same. This can be understood in a one-electron picture: both types of oscillations are actually governed by the same area bounded for instance, by the $3p\pi$ and $4d\pi$ MO's.

E. Scattering calculations

The experimentally determined differential cross sections at 2 keV were shown in Fig. 5. The aim of this section is to obtain information from these experimental data about the molecular energy levels of the $(Na\text{-}Ne)^{+}$ system. It is, of course, impossible to attempt to obtain precise shapes of an infinite number of molecular energy levels from a relatively small amount of experimental data. Thus, to make the problem tractable, all singly excited molecular states, which form a relatively narrow band of energies (the A series of Fig. 14), will be replaced by a single representative singly excited state. Similarly, the C series of Fig. 14 which constitutes the infinite number of doubly excited states will be replaced by a single representative doubly excited state. Together with the ground electronic state, there are thus three molecular energy curves which will be fitted by the experimental data. These are illustrated in Fig. 18. The ground-state energy is fitted by the potential of Kita *et al.*[19]

$$V_0(R) = 196.7 \exp(-2.71R) \text{ a.u.}$$

over the entire range of internuclear separations

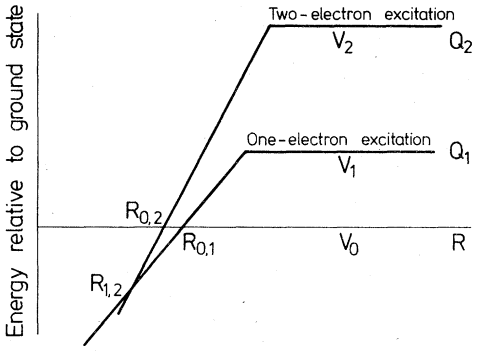

FIG. 18. Simplified model of molecular potentials. The energy differences $V_1 - V_0$ and $V_2 - V_0$ are approximated by linear functions of internuclear separation R with slopes S_1 and S_2, respectively, up to the points where they intersect the respective excitation energies of the separated systems. Beyond these intersections, the potentials are taken to be constants, with values Q_1 and Q_2. The elastic potential is represented by V_0, while representative potentials which separate as singly and doubly excited states are denoted by V_1 and V_2. Finally, $R_{n,m}$ represents the crossing radius of V_n with V_m. The model molecular potentials should be compared with the *ab initio* calculations shown in Fig. 16, A and C series.

R for which elastic collisions have any appreciable probability. Further, as shown in Fig. 18, the energy differences between ground and excited states are approximated by the piecewise linear functions

$$V_1 - V_0 = \begin{cases} (R - R_{0,1})S_1 & \text{for } R \leq R_{0,1} + Q_1/S_1 \\ Q_1 & \text{for } R \geq R_{0,1} + Q_1/S_1 ; \end{cases} \tag{5a}$$

$$V_2 - V_0 = \begin{cases} (R - R_{0,2})S_2 & \text{for } R \leq R_{0,2} + Q_2/S_2 \\ Q_2 & \text{for } R \geq R_{0,2} + Q_2/S_2 . \end{cases} \tag{5b}$$

As can be seen in Fig. 18, Q_1 and Q_2 are the excitation energies of the representative singly and doubly excited molecular states at $R = \infty$, while $R_{0,1}$ and $R_{0,2}$ locate the curve crossings of the elastic potential V_0 with the potential curves V_1 and V_2 for singly and doubly excited states.

Finally, S_1 and S_2 give the slopes of the energy differences $V_1 - V_0$ and $V_2 - V_0$. The four adjustable parameters S_1, S_2, $R_{0,1}$, and $R_{0,2}$, together with Q_1 and Q_2, determine $V_1 - V_0$ and $V_2 - V_0$ in this simplified molecular potential model. The location of the last level crossing $R_{1,2}$ is not an independent parameter; it is determined by S_1, S_2, $R_{0,1}$, and $R_{0,2}$. Moreover, Q_1 and Q_2 are not considered adjustable parameters; they are fixed by the respective atomic excitation energies ($Q_1 = 0.6$ a.u., $Q_2 = 2.0$ a.u.). The two remaining adjustable parameters, making up the total of six, are the two needed to specify the Born-Mayer potential which approximates the elastic poten-

tial V_0. Calculations show that the precise shapes of the energy curves at larger internuclear separations are not of much importance in determining the deflections. At these larger separations, the radial direction and the direction of motion nearly coincide. As a consequence, the interatomic forces have only small transverse components and cannot, therefore, significantly affect the scattering. Thus, the difference between the smooth variation of the actual molecular potentials with internuclear separation and the piecewise linear approximations are not significant. The approximations (5) are not essential to the method; they are important only to reduce the number of parameters which can be extracted from a relatively small amount of data.

With these three potentials, six channels are considered as illustrated in Fig. 19: one elastic channel, designated by *ee*; three channels which results in single electron excitations, designated by *es*, *ss*, and *ds*, depending on whether the scattering follows the elastic, singly excited, or doubly excited potentials on the incoming portion of the trajectory; and finally, two channels which results in doubly excitations, designated by *sd* and *dd*. A "channel" represents a specification of potentials on the incoming and outgoing portions of the trajectory. Each channel, therefore, has its own particular deflection function, $\tau_i(b)$ and they are all different. Letting i stand for any one of the channels enumerated above, the deflection $\tau = E\theta(b)$ is obtained from the equation

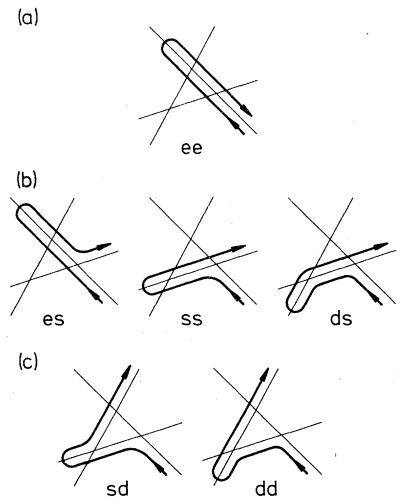

FIG. 19. The six channels for which ρ vs τ were calculated: (a) elastic scattering, (b) one-electron processes, and (c) two-electron processes. These were then used to fit the experimental data by adjustment of the potential parameters of the simplified model. The respective probabilities for each channel was also obtained in the fitting process.

$$\theta(b) = \pi - \int_0^{u_m} du\,[(b^{-2} - u^2 - 2mW_{\text{in}}/L^2)^{-1/2} + (b^{-2} - u^2 - 2mW_{\text{out}}/L^2)^{-1/2}],$$

where θ is the scattering angle, b the impact parameter, $u = 1/R$, $u_m = 1/R_{\text{min}}$, and L the angular momentum. W_{in} and W_{out} are the molecular potential curves on the respective portions of the trajectory. This is valid in both the classical and semi-quantum-mechanical treatments.[48]

The deflection function is inverted to yield $b_i(\tau)$, the impact parameter which results in the specified deflection τ when the forces are those defined by the ith channel. Over the range of impact parameters for which the collision is essentially classical for the ith channel, the ρ_i's are obtained from

$$\rho_i(b_i(\tau)) = b\tau_i/(d\tau_i/db).$$

However, for impact parameters near the onset of an excitation or in the vicinity of a sign reversal of $d\tau_i/db$ (i.e., a rainbow maximum), a semiquantal treatment[48] is required for the differential cross section and was done. For this system, rainbow maxima regions overlapped the regions of excitation onset, and the Airy function approximation of Ford and Wheeler[49] was inapplicable. As a check, both the classical and semiquantal calculations for each ρ_i were carried out over the entire range of impact parameters. The semiquantal results nicely reduced to the classical results (on which were superimposed small rapid diffraction oscillations) in those regions of b which are removed from an onset or rainbow region by more than the Heisenberg Δb, where $p\,\Delta b\,\Delta\theta \geq \hbar$. Neglecting interference effects (Stueckelberg oscillations), an attempt is then made to fit the experimental ρ vs τ curves by empirically adjusting the channel probabilities $p_i(b)$ that the system will follow the ith channel when the projectile is incident at impact parameter b. Clearly, for each given impact parameter, some channel must be followed, so that

$$\sum_i p_i(b) = 1, \quad p_i \geq 0. \tag{6}$$

It is important to note that the probabilities at fixed reduced scattering angle τ do *not* add up to unity, since collisions with several impact parameters can result in the same deflection. The fitting should be such that

$$p_{ee}\,\rho_{ee} = \rho_e^{\text{expt}}(\tau), \tag{7a}$$

$$p_{es}\,\rho_{es} + p_{ss}\,\rho_{ss} + p_{ds}\,\rho_{ds} = \rho_s^{\text{expt}}(\tau), \tag{7b}$$

$$p_{sd}\,\rho_{sd} + p_{dd}\,\rho_{dd} = \rho_d^{\text{expt}}(\tau), \tag{7c}$$

where p_i and ρ_i are determined as functions of

τ from the inverse of the ith deflection function $b_i(\tau)$. This is necessary because the experimental quantities on the right-hand side of Eq. (7) are known only as functions of scattering angle τ.

Superficially, it might appear that for arbitrary potential curves, the three experimental functions $\rho_i^{\text{expt}}(\tau)$ could always be fitted by six adjustable functions, the channel probabilities. Such, however, is not the case. The two conditions (6) impose severe restrictions.

The results are given in Figs. 20 and 21. Figure 20 shows a comparison between the experimental curves and the fit obtained following the procedure outlined above. The experimental curve for one-electron excitation is obtained by adding the curves B and B' of Fig. 5; the two-electron excitation curve is similarly obtained from addition of curves C and C'. The corresponding channel probabilities are shown in Fig. 21, as function of $R_{\min}$.

The experimental fit clearly and unambigously fixes the location of the first crossing $R_{0,1}$ at 1.63 a.u., in agreement with the *ab initio* calculations. The slope S_1 as determined by the experimental fit, is also in agreement with the calculations. However, the experimental fit is not sufficiently sensitive to add much information. With $R_{0,1}$ and Q_1 already determined, any *reasonable* estimate of the point of which the singly excited molecular energy curve flattens out to the separated-atom limit, would yield a slope S_1 which could be fit to the experiment about as well. The crossing $R_{0,2}$ cannot be determined by experiment since there is very little transition probability at this point. The experimental value for $R_{1,2}$ is found to be 1.39 a.u., which is slightly smaller than the value of 1.44 a.u. obtained in the *ab*

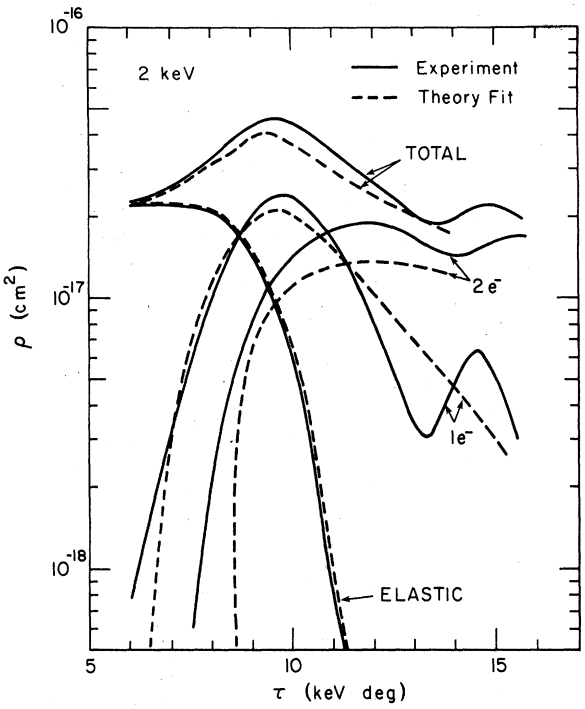

FIG. 20. Comparison between "theory" and experiment. The solid lines show the experimental ρ vs τ reduced differential cross sections. For both single and double excitation processes, the direct and exchange contributions from Fig. 5 have been combined to give the experimental curves shown. The broken lines show the best fit obtainable with the simplified molecular potential model and the six channels used. The dotted curve shows the reduced differential cross section which follows from the potential of Kita *et al.*

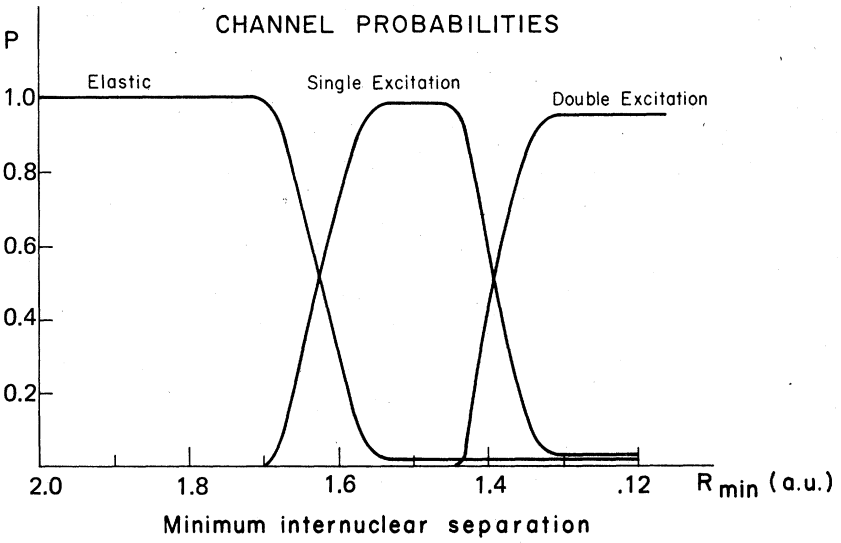

FIG. 21. Channel probabilities which yield the best fit with the experimental data. All three channels which lead to single-electron excitation have been combined into a single curve, as have all channels leading to double-electron excitation.

initio calculations. Again, the experimental fit is not extremely sensitive to the slope S_2. However, a 30% reduction in S_2 from that given by the *ab initio* calculations yields a small but detectably poorer fit with experiment.

Fortunately, a considerable more sensitive probe of the slope S at a crossing is the period of the Stueckelberg oscillations that show up in the inelastic channel, due to the phase difference between the scattering amplitudes for the two different paths leading to the excited channel. By attributing numbers $N(E,\theta)$ to the maxima and minima of these experimentally observed oscillations in the inelastic channel (Fig. 7) one may calculate the reduced action $a(\tau)$ by the following relation[50]

$$a(\tau,E)=2\pi\hbar(E_{\text{c.m.}}/2\mu)^{1/2}[N(E,\tau)+\tfrac{1}{4}]. \tag{8}$$

Here μ is the reduced mass and $E_{\text{c.m.}}$ the energy in the center of mass frame. The difference Δb in impact parameter for the two paths leading to the same scattering angle θ is equal to the slope of this curve

$$\Delta b(\tau)=\frac{d}{d\tau}\,a(\tau).$$

Figure 22 presents the analysis of the Stueckelberg oscillations observed in the one-electron excitation channel (Fig. 7). The slope Δb is almost constant in this τ range and about equal to 0.092 a.u. This slope is approximately reproduced assuming a slope at the X-A crossing of $S_1=3.0$ a.u. Changing S_1 by ± 0.5 a.u. yields a noticable change in the corresponding Δb's, as indicated by the two dotted lines. The frozen orbital (FO) method thus slightly overestimates the slope at the crossing, as expected for this theoretical approach.

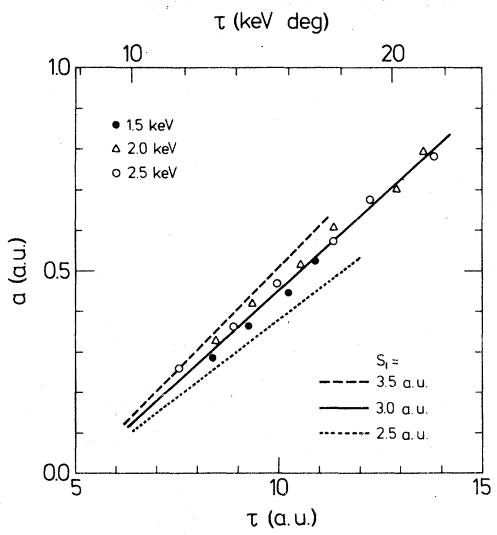

FIG. 22. Analysis of the maxima and minima of the Stueckelberg oscillations observed in the one-electron excitation channel, Fig. 7. The reduced action is plotted vs the reduced scattering angle, cf. Eq. (8). A value of the slope S_1 at the first crossing (Fig. 18) of about 1.5 a.u. is consistent with the observed spacing of the oscillations.

TABLE V. Comparison of crossing radii and potential-energy curve slopes in a.u., as obtained from theory and analysis of the experimental results, as illustrated in Figs. 20 and 22.

	Crossing radii			Slopes	
	$R_{0,1}$	$R_{1,2}$	$R_{0,2}$	S_1	S_2
Ab initio theory	1.63	1.44	1.54	3.7	6.9
Scattering analysis	1.63	1.39	•••	3.7	6.9
Stueckelberg analysis	•••	•••	•••	3.0	•••

Unfortunately, the Stueckelberg oscillations in the two-electron excitation channel are not sufficiently developed to warrant a similar analysis. Therefore, for the evaluation of the probabilities of Fig. 21 the slopes of the FO method have been used for consistency. Minor changes of the slopes do not influence the probabilities significantly.

The parameters obtained from experiment are presented in Table V.

F. Structure in the toal differential cross section

The widely held conception of large-angle atom-atom (or ion-atom) collisions at keV energies is that of a screened Coulomb scattering process, with a functional relation between impact parameter b and reduced scattering angle τ. It is, of course, expected that the partial cross section for any given final state will show structure in the differential cross section, reflecting the variation of probability of the given final state with impact parameter. However, it is generally believed that the overall differential cross section, the sum over all final states, should be smooth, as determined by the deflection $\tau(b)$ for the screened Coulomb potential.

Thus, it is intriguing and worthy of explanation when rather dramatic structure is found in the overall differential cross section. These have been attributed to quantum-mechanical interference effects (Marchi[51]) and to rainbow maxima in the differential cross section at minima in a channel deflection function (Marchi[51] and Afrosimov *et al.*[52]). However, when the differential cross section is analyzed in terms of it's individual components, as done in subsection E above, a third cause for structure in the overall differential

cross section is clearly evident. In the $(Na\text{-}Ne)^+$ system, this third mechanism proves to be the dominant cause for the structure. The reason for the structure is as follows:

In the repulsive scattering region, electronic excitation *always produces a shift in scattering angle toward smaller scattering angles*. Therefore, in the vicinity of an excitation threshold, the ρ vs τ curve for the more highly excited state is shifted back so that it overlaps that for the less excited state. In effect, collisions from two different impact parameters are appearing at the same value of τ, producing a bump in the differential cross section. It is to be noted that a minimum in the deflection function also causes a pileup at one particular value of τ from collisions from a range of impace parameters.

VIII. CONCLUSIONS

A. Consistent interpretation

The results of the present investigation of low-energy Na^+-Ne collisions are succinctly summarized in Fig. 23. In collisions for which the distance of closest approach R_{min} is larger than about 1.63 a.u. the scattering is purely elastic. However, as soon as R_{min} becomes smaller than 1.63 a.u. the probability for excitation is almost unity. If $1.39 < R_{min} < 1.63$ only one $2p$ electron is excited ($4f\sigma$ promotion) and predominantly to either a Ne($3p$) level or transferred to the Na($3p$) level; these processes give rise to photon emission exhibiting Rosenthal oscillations. If $R_0 < 1.39$ a.u., excitation of two $2p$ neon electrons dominates, feeding effectively four major groups of exit channels: (a_1) transfer of one electron to the projectile with simultaneous excitation of a neon level; or (a_2) doubly excited autoionizing neon levels; or—following a core L-vacancy sharing process, which transfers one of the Ne $2p$ vacancies to the Na $2p$ subshell—either (b_1) simultaneous excitation of one electron of both collision partners, or (b_2) excitation of autoionizing levels in neutral sodium plus a Ne^+ ion in the ground state. The two latter channels exhibit Rosenthal interferences giving rise to oscillations in the cross sections for electron emission which match oscillations observed in the photon spectrum. A major fraction of the violent collisions produces excitation of electrons to continuum states. No violation of the Wigner spin-conservation rule was required in the above interpretation. In the separated-atom limit, of course, spin-orbit effects have to be taken into account in the way done by Tolk *et al.*

Based on a consistent set of experimental data, accurate *ab initio* calculations were performed and have yielded detailed information on the molecular potential curves of the $(Na\text{-}Ne)^+$ system, including locations of the important curve crossings and the magnitude of the interaction matrix elements at the crossings. These results have provided a basis for a detailed interpretation of the more spectacular of the experimental findings, including in many cases quantitative estimates of cross sections or cross-section ratios for the often complicated multistep processes that show up in the different regions in Fig. 23. Finally, scattering calculations based on a simplified model of the important molecular curves have confirmed the consistency between the theoretical potential curves and the experimental differential cross sections, and strikingly corroborated the schematic overall picture of the collision presented in Fig. 23.

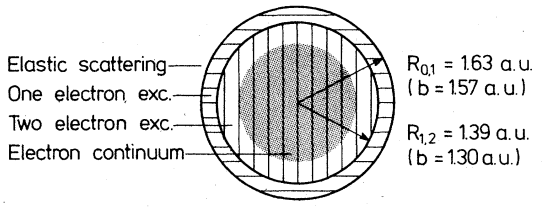

FIG. 23. Schematic picture of the impact-parameter dependence and absolute cross sections for the excitation processes in 1–10 keV Na^+-Ne collisions. For a discussion, see the text.

B. Pitfalls

In the introduction it was claimed that a consistent interpretation is only possible with a combined effort of various experimental and theoretical approaches. Looking back, we can strongly justify this statement by demonstrating in a few examples how any single experimental technique taken alone can yield results that are misleading.

(i) uv spectroscopy shows strong emission from Ne($3s$), Ne^+($3s$), and Na^+($3s$) levels. However, the Ne($3s$) emission is mainly a secondary process, with the initial event being a Ne($3p$) excitation which cascades to the Ne($3s$) level by emission of a photon in the visible wavelength range. Similarly, the Ne^+($3s$) emission is, to a large extent, also a secondary process; it is caused by the excitation of the $Ne(^1D)3p^2\,^1L$ level, which decays to the $Ne^+(^1D)3s$ level by emission of a low-energy electron. Finally, the observation of Na^+ emission does not reveal the crucial fact that Na^+ excitation only takes place with simultaneously excitation of Ne, as demonstrated by the energy-loss measurements.

(ii) Photon spectroscopy in the visible range shows considerable excitation of neon levels with predominantly triplet character. Neglect of two-

electron processes must lead to the conclusion that the Wigner spin-conservation rule has been violated. The energy-loss spectra show, however, that two-electron processes are indeed important, and analysis of results from the electron spectra and uv spectra shows that simultaneous triplet excitation of both target and projectile may very well account for the observed triplet excitation, without invoking violation of spin conservation.

(iii) Electron spectroscopy alone, without reference to the MO model, may lead to wrong assignments of the observed lines; even if the assignments are correct, the $Ne(^1D)3p\,^2{}^1L$ excitation is not observed. However, both the MO model and the energy-loss spectra strongly suggest its presence, and the paradox is solved by observation of the strong $Ne^+(^1D)3s$ emission in the uv spectrum.

(iv) Differential energy loss analysis and the time-of-flight measurements in most cases do not reveal the details of the one- and two-electron processes. Even worse, the production of autoionizing neutral sodium levels, though it is an important exchange process, contributes nevertheless to the two-electron excitation peak observed in the direct channel, since these atoms autoionize before detection. However, the correct information is obtained from the electron spectra.

C. Final remarks

It may thus be concluded that for collision systems where several excitation mechanisms are active, giving rise to a complicated assortment of exit channels, a consistent picture can only be safely constructed by combining information from different experimental techniques (differential energy-loss measurements, photon and electron spectroscopy). It is, however, gratifying to experience that when this is done, even a complicated many-channel process can indeed by interpreted in detail in terms of succesive actions of the well-known mechanisms encountered previously in simpler collision systems.

ACKNOWLEDGMENTS

We would like to thank J. P. Gauyacq and F. Masnou-Seeuws for useful discussions. One of us (N.A.) wishes to acknowledge travel support from the Danish Natural Science Research Council and from Institut Français, Copenhagen.

---

*Also at Centre de Mecanique Ondulatoire Appliquée, 23 rue de Maroc, F-75019, Paris, France.

†On leave from Department of Physics, University of Connecticut, Storrs, Conn. 06268.

[1]C. Ramsauer and O. Beeck, Ann. Phys. (Leipz.) 87, 1 (1928).

[2]R. M. Sutton and J. C. Mouzon, Phys. Rev. 37, 379 (1931).

[3]W. Weizel and O. Beeck, Z. Phys. 76, 250 (1932).

[4]E. C. G. Stueckelberg, Helv. Phys. Acta 5, 369 (1932). The discussion of the K^+-Ar collisions is found in Sec. 15.

[5]O. Beeck, Phys. Z. 35, 36 (1934).

[6]W. Maurer, Z. Phys. 101, 323 (1936).

[7]J. C. Mouzon, Phys. Rev. 41, 605 (1932).

[8]J. Østgaard Olsen and T. Andersen, J. Phys. B 8, L421 (1975).

[9]T. Andersen, A. K. Nielsen, and K. J. Olsen, Phys. Rev. Lett. 31, 739 (1973); Phys. Rev. A 10, 2174 (1974).

[10]B. Fastrup, G. Hermann, and K. J. Smith, Phys. Rev. A 3, 1591 (1971).

[11]J. C. Brenot, J. Pommier, D. Dhuicq, and M. Barat, J. Phys. B 8, 448 (1975).

[12]O. Heinz and R. T. Reaves, Rev. Sci. Instrum. 39, 1229 (1968).

[13]M. Barat, in *Proceedings of the Eighth International Conference on the Physics of Electronic and Atomic Collisions*, Invited Lectures, edited by B. C. Čobić and M. H. Kurepa (Institute of Physics, Belgrade, 1973), p. 43.

[14]P. Dahl, M. Rødbro, B. Fastrup, and M. E. Rudd, J. Phys. B 9, 1567 (1976).

[15]V. V. Afrosimov, Yu. S. Gordeev, V. M. Lavrov, and V. K. Nikulin, in *Proceedings of the Seventh International Conference on the Physics of Electronic and Atomic Collisions*, Abstracts of Papers, edited by L. M. Branscomb *et al.* (North-Holland, Amsterdam, 1971), pp. 143–145; V. V. Afrosimov, Yu. S. Gordeev, and V. M. Lavrov, in Ref. 13, pp. 190–191.

[16]J. C. Brenot, D. Dhuicq, J. P. Gauyacq, J. Pommier, V. Sidis, M. Barat, and E. Pollack, Phys. Rev. A 11, 1245 (1975).

[17]V. V. Afrosimov, S. V. Bobashev, Yu. S. Gordeev, and V. M. Lavrov, Zh. Eksp. Teor. Fiz. 62, 61 (1972) [Sov. Phys. JETP 35, 34 (1972)]. V. V. Afrosimov, Yu. S. Gordeev, and V. M. Lavrov, Zh. Eksp. Teor. Fiz. 68, 1715 (1975) [Sov. Phys. JETP 41, 860 (1976)].

[18]F. T. Smith, R. P. Marchi, W. Aberth, and D. C. Lorents, Phys. Rev. 161, 31 (1967).

[19]S. Kita, K. Noda, and H. Inouye, J. Chem. Phys. 63, 4930 (1975).

[20]J. Baudon, M. Barat, and M. Abignoli, J. Phys. B 3, 207 (1970).

[21]Yu. F. Bydin, V. A. Vol'pyas, and V. I. Ogurtsov, Pis'ma Zh. Eksp. Teor. Fiz. 18, 547 (1973) [JETP Lett. 18, 322 (1973)].

[22]J. Østgaard Olsen and N. Andersen, J. Phys. B 10, 101 (1977); N. Andersen and J. Østgaard Olsen, *ibid.* 10, L719 (1977).

[23]D. J. Pegg, H. H. Haselton, R. S. Thoe, P. M. Griffin, D. M. Brown, and I. A. Sellin, Phys. Rev. A 12, 1330 (1975); P. Dahl, M. Rødbro, G. Hermann, B. Fastrup, and M. E. Rudd, *ibid.* 9, 1581 (1976); E. Brueckmann, B. Breuckmann, W. Melhorn, and W. Schmitz, *ibid.* 10, 3135 (1977).

[24]J. Østgaard Olsen and N. Andersen, in *Proceedings of the Eighth International Summer School and Symposium on the Physics of Ionized Gases*, Contributed Papers, edited by B. Navinšek (J. Stefan Institute, University of Ljubljana, 1976), pp. 94a–96.
[25]J. M. Sichel and J. Langlois (private communication).
[26]V. P. Belik, S. V. Bobashev, and S. P. Dmitriev, Zh. Eksp. Teor. Fiz. 67, 1674 (1974) [Sov. Phys. JETP 40, 833 (1975)].
[27]S. V. Bobashev and V. A. Kharchenko, in *Proceedings of the Tenth International Conference on the Physics of Electronic and Atomic Collisions*, Abstracts of Papers, edited by M. Barat and J. Reinhardt (Commissariat a l'Energie Atomique, Paris, 1977), pp. 964–965.
[28]N. H. Tolk, C. W. White, S. H. Neff, and W. Lichten, Phys. Rev. Lett. 31, 671 (1973); N. H. Tolk, J. C. Tully, C. W. White, J. Kraus, A. A. Monge, D. L. Simms, M. F. Robbins, S. H. Neff, and W. Lichten, Phys. Rev. A 13, 969 (1976).
[29]S. V. Bobashev, Pis'ma Zh. Eksp. Teor. Fiz. 11, 389 (1970) [JETP Lett. 11, 260 (1970)].
[30]J. Østgaard Olsen, N. Andersen, and T. Andersen, J. Phys. B 10, 1723 (1977).
[31]E. E. Nikitin, M. Ya. Ovchinnikova, and A. I. Shushin, Zh. Eksp. Teor. Fiz. 70, 1243 (1976) [Sov. Phys. JETP 43, 646 (1976)]; P. J. Martin, G. Riecke, J. Hermann, L. Zehnle, and V. Kempter, J. Phys. B 11, 1991 (1978) found for the isoelectronic Ne-Ne system at collision energies comparable to ours, that 25% of the Ne($3p$) excitation is due to simultaneous excitation.
[32]W. Lichten, Phys. Rev. 164, 131 (1967).
[33]J. P. Gauyacq, J. Phys. B 11, 85 (1978).
[34]C. C. I. Roothaan, Rev. Mod. Phys. 23, 69 (1951).
[35]P. S. Bagus, B. Liu, A. D. McLean, and M. Yoshimine of the theoretical chemistry group at the IBM Research Institute in San José, Calif. Preliminary descriptions of the ALCHEMY program are given by A. D. McLean [in *Proceedings of the Conference on Potential Energy Surfaces in Chemistry* (California, University, Santa Cruz, 1970)] and by P. S. Bagus [in *Selected Topics in Molecular Physics* (Springer, Berlin, 1972)]. See also IBM Research publication No. 14, p. 748 (1971).
[36]L. Ya. Efremenkova, A. A. Radsig, and B. M. Smirnov, Opt. Spektrosk. 36, 61 (1974) [Opt. Spectrosc. 36, 35 (1974)]. The analytical formula for the potential should be corrected, according to F. Masnou-Seeuws, M. Phillippe, and P. Valiron, J. Phys. B (to be published).
[37]N. A. Sondergaard and E. A. Mason, J. Chem. Phys. 62, 1299 (1975).
[38]B. M. Smirnov, *Asymptotic Methods in the Theory of Atomic Collisions* (Atomizdat, Moscow, 1973).
[39]The energy of the relevant Ne($\pi 2p^4\sigma 2p\pi 3p$)^1 state has been evaluated using the transformation matrices given in Ref. 28.
[40]Yu. N. Demkov, Zh. Eksp. Teor. Fiz. 45, 195 (1963) [Sov. Phys. JETP 18, 138 (1964)].
[41]H. Rosenthal and H. M. Foley, Phys. Rev. Lett. 23, 1480 (1969); H. Rosenthal, Phys. Rev. A 4, 1030 (1971).
[42]V. Sidis, N. Stolterfoht, and M. Barat, J. Phys. B 10, 2815 (1977).
[43]J. P. Gauyacq, J. Phys. B 9, 2289 (1976).
[44]W. E. Mayerhof, Phys. Rev. Lett. 31, 1341 (1973).
[45]A value of the coupling matrix element $H_{BC} \sim 0.05$ a.u. for the K^+-Ar system yields $p \sim 30\%$, the experimental value. Strong support for this interpretation is also obtained from a comparison of the differential cross sections of Afrosimov *et al.* (Ref. 17) for $K^+(4s)$ and $K^+(4p)$ excitation, respectively: The $K^+(4s)$ DCS has a structure similar to the Ar($4s^2$) *two*-electron excitation, but different from the Ar one-electron excitation DCS. The $K^+(4p)$ DCS has a structure similar to the Ar($4s4p$, $4p^2$) *two*-electron excitation, showing that the primary excitation mechanism is the same for these two channels.
[46]N. Stolterfoht and U. Leithäuser, Phys. Rev. Lett. 36, 186 (1976).
[47]Among all states corresponding to the Na($2p^5 3s 3p$) configurations, only the Na($2p^5[3s3p\ (^1P)]^2P$) state can directly be populated by the feeding molecular state. Evidence for this selection rule is given by the observation of this line only (peak E in Fig. 9). This independent confirmation of the assignement of Breuckmann *et al.*, Ref. 23, shows again that low-energy heavy-particle collisions provide a powerful tool for identification of autoionizing spectral lines, cf. Ref. 22.
[48]N. F. Mott and H. S. W. Massey, *The Theory of Atomic Collisions*, 2nd ed. (Clarendon, Oxford, 1949).
[49]K. W. Ford and J. A. Wheeler, Ann. Phys. (N.Y.) 7, 259 (1959).
[50]F. T. Smith, H. H. Fleischmann, and R. A. Yong, Phys. Rev. A 2, 379 (1970).
[51]R. P. Marchi, Phys. Rev. 183, 185 (1969).
[52]V. V. Afrosimov, Yu. S. Gordeev, V. K. Nikulin, A. M. Polyanskii, and A. P. Shergin, Zh. Eksp. Teor. Fiz. 62, 848 (1972) [Sov. Phys. JETP 35, 449 (1972)].